$r = 20\ R_J$ and decreases markedly with increasing distance, though nowhere near as fast as the $1/r^3$ dependence looked for in Section 11.3.2; $h_{max}$ approaches zero, of course, at $r = r_{nl}$ where $B_z \to 0$. Equation (11.105) predicts a simple power-law dependence $h_{max} \sim 1/r^{1-a} = 1/r^{0.3}$, a rather slow decrease cited by Goertz [1976b] and Thomsen and Goertz [1981a] as being close to a constant thickness originally assumed in the model; that advantage, as we have seen, has been bought at the price of significantly modifying $B_z$ and eliminating the identification of open field lines that was given much emphasis in the original model [Goertz et al., 1976; see also Fig. 10.11 and its caption]. (It may be pointed out, though, that the last closed field line in the original model is identified by its equatorial crossing at $r = r_{nl}$, the location of the neutral line, and since $r_{nl}$ lies well outside the model's range of applicability the significance of the identification is perhaps doubtful in any case.)

To calculate actual values of $h$ and not just $h_{max}$, assumptions about the quantity $\mu$ must be made. Goertz [1976b] assumed that $\mu$ was a constant and set $V_\phi^2/w^2 = 2$; his $h$ is simply scaled down from $h_{max}$ by a constant factor. Liu [1982] assumed that $V_\phi = \omega r$ with $\omega \sim 1/r^2$, derived from a model of partial corotation (see Sec. 11.4.4), and that $w^2 \equiv P/\rho$ is obtainable from a relation $P \sim \rho^\gamma$ with $P$ given by pressure balance with the magnetic field. He treated the adiabatic ($\gamma = 5/3$) and isothermal ($\gamma = 1$) cases with several different initial ratios $V_\phi^2/w^2$ specified at the reference distance $r = 20\ R_J$, obtaining a number of $h$ vs. $r$ profiles which all lie under the $h_{max}$ vs. $r$ curve of Figure 11.9, of course, and generally decrease with increasing $r$, although for the isothermal case with $V_\phi^2/w^2 > 1.72$ he finds that $h$ initially increases with increasing $r$ and reaches a maximum before decreasing.

Theoretical estimation of the thickness of the current sheet and its dependence on the distance is thus at present rather uncertain. There is no unique model, in large part because of still unresolved uncertainties about the magnetic field, particularly its $B_z$ component, and inability to decide among several still viable hypotheses about the ratio of plasma thermal speed to azimuthal flow speed.

### 4. Azimuthal magnetic fields and angular momentum transfer

So far in this chapter, the azimuthal (or nonmeridional or toroidal) magnetic field component $B_\phi$ has been neglected, partly on the grounds that it is relatively small and partly because it plays no direct role in the stress balance along the radial and normal directions. However, the existence of well-defined large-scale azimuthal magnetic fields which, in the outermost regions of the magnetosphere, can become comparable in magnitude to the other field components, is a prominent feature of the observations. The interpretation of these fields has become a matter of considerable controversy, involving some fundamental questions about the physics of the Jovian magnetosphere, in particular about the relative roles of rotation, plasma outflow, and solar wind effects. Chapter 1, Section 1.3 contains a brief account, with references, of the observations and models (presented, however, entirely from the point of view of one side in the controversy).

With $\hat{\phi}$ defined as positive in the direction of corotation, the observed $B_\phi$ is negative in regions above the current sheet and positive below; within the current sheet $B_\phi$ is greatly reduced in magnitude, consistent with its required reversal. Looked at from above the pole, the magnetic field lines thus have a spiral appearance of lagging behind the planetary rotation. Such a configuration is readily interpreted as a rotation-associated effect, a "wrapping up" of the field lines as the plasma in the outer magnetosphere is slowed down in its azimuthal motion, either by a tangential drag between it and the solar wind or by its own inertia if it is moving radially outward. Theoretical suggestions



of the lagging spiral configuration and of both these possible explanations were made [Piddington, 1969] long before there were any in situ observations. Implicit in this interpretation is the assumption that the azimuthal field pattern has the same character all around the planet, that is, the sign of $B_\phi$ is, for the most part, independent of local time, although a local-time dependence of the magnitude of $B_\phi$ is not precluded. The dominant mechanical effect of the stresses in the magnetic field is a *torque* opposed to the planetary rotation and extracting energy from it.

An alternative interpretation, championed principally by Ness and his coworkers [Ness et al., 1979a,b,c; Behannon, Burlaga, and Ness, 1981; Chap. 1], considers the azimuthal fields to be primarily associated not with Jupiter's rotation but with its interaction with the solar wind; the observed $B_\phi$ is ascribed to the bending of magnetic field lines away from the Sun by the action of a solar-wind-aligned magnetospheric tail, similar to what is observed in the terrestrial magnetosphere [e.g., Fairfield, 1968], and the resemblance to the rotationally lagging spiral is viewed as merely the result of the coincidental fact that all the available observations have been made in the postmidnight–dawn–prenoon side of the Jovian magnetosphere. Implicit in this interpretation is the assumption that the azimuthal magnetic fields in the yet unobserved dusk side also point away from the Sun, that is, $B_\phi$ reverses sign at or near the noon–midnight meridian. To first approximation, the magnetic torques from the dawn and dusk sides cancel; the dominant mechanical effect of the stresses in the magnetic field is now not a torque but a *force* in the direction of solar wind flow (see discussions of the terrestrial analog by Siscoe [1966], Siscoe and Cummings [1969], and Carovillano and Siscoe [1973]).

It is obvious that observations during even a single traversal of the outer magnetosphere in the premidnight or dusk local time sector should settle the controversy conclusively because the two interpretations firmly predict opposite signs for $B_\phi$ there. However, spacecraft missions with the required trajectories have not been flown yet, and the interpretation of $B_\phi$ (only observed in regions where both models predict the same sign) remains in dispute. On one side, many details of magnetic field observations have been fitted into the framework of the solar-wind-aligned magnetotail interpretation, as summarized in Chapter 1, Sections 1.3 and 1.4 (although the impression given there, that the controversy is as good as settled in favor of this model, is the personal opinion of the chapter's authors and does not represent a consensus). On the other side, Vasyliunas and Dessler [1981] argue that an Earthlike magnetotail can have significant effects only in regions where the magnetic pressure is at least an order of magnitude lower than the solar wind ram pressure, hence at distances no closer than 80–100 $R_J$ in the nightside Jovian magnetosphere (see also Sec. 11.3.5). Recently, Vasyliunas [1982a] has reexamined the magnetic field evidence adduced for a Jovian magnetotail and concluded that it is equally consistent with the rotational interpretation (the "wrapped-around magnetotail" in the phrasing of Piddington [1969]); he also finds that the terrestrial analog predicts a local-time variation of $B_\phi$ not seen at Jupiter.

In the midnight-to-dawn sector, the region traversed by the outbound passes of Pioneer 10, Voyager 1, and Voyager 2, the quantitative description of the observed $B_\phi$ is relatively simple. Goertz et al. [1976] found that Pioneer 10 observations of $B_\phi$ could be fitted by the form (in cylindrical coordinates)

$$B_\phi/rB_r = (1/r_f)\,F(r) \tag{11.107}$$

where $r_f = 160\ R_J$ is a constant and $F(r)$ is a slowly varying function nearly equal to unity; Goertz et al. obtained as the best fit

$$F(r) = \exp(r/500\ R_J) \tag{11.108}$$

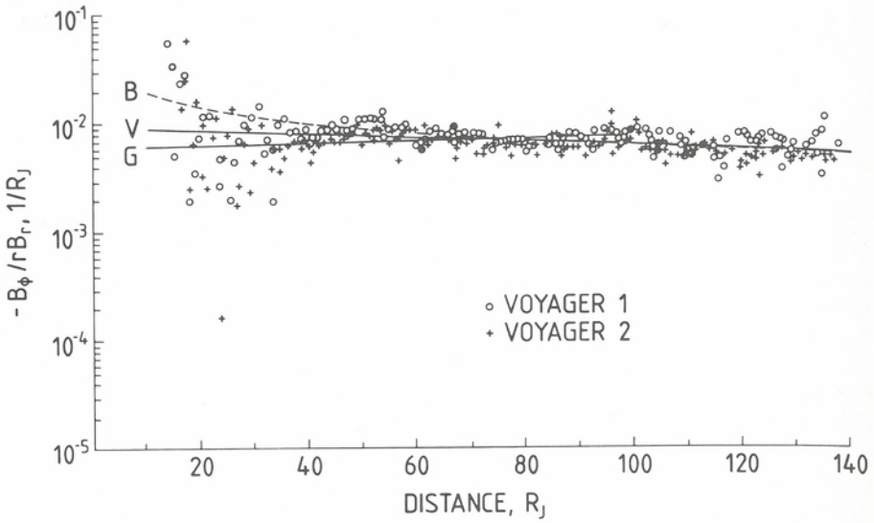


Fig. 11.10. The ratio $B_\circ/rB_r$ observed during the Voyager 1 and 2 outbound passes [from Figs. 11 and 12 of Behannon, Burlaga, and Ness, 1981, with omission of measurements within the current sheet and the depressed field region]. The lines are various empirical fits: G represents Equation (11.108) (drawn over the radial range of Pioneer 10 observations only), B is Equation (11.109) and V is Equation (11.110).

which varies from 1.04 to 1.17 over the distance range 20 to 80 $R_J$ of the observations. Behannon, Burlaga, and Ness [1981] found a very similar result from Voyager 1 and 2 observations: $B_\circ$ given by Equation (11.107) but with a somewhat different $F(r)$; with the choice $r_J = 160\ R_J$ again, the fit of Behannon, Burlaga, and Ness is

$$F(r) = (100\ R_J/r)^{1/2} \tag{11.109}$$

which decreases from 2.24 at 20 $R_J$ to 0.845 at 140 $R_J$. In both cases, the result applies only outside the current sheet region; inside it, $B_\circ$ may be significantly reduced in magnitude from the value given by (11.107). The fact that $B_\circ/rB_r$ appears to be nearly constant or only slowly decreasing has played a major role in the interpretation of the observed azimuthal field, as discussed further on.

Figure 11.10 shows $B_\circ/rB_r$ outside the current sheet as a function of radial distance: the combined Voyager 1 and 2 observations and the fitted curve representing the Pioneer 10 observations, together with other suggested fits, Equation (11.109) and my own suggestion

$$F(r) = 1.44 \exp -(r/260\ R_J) \tag{11.110}$$

Except at distances $r < 40\ R_J$, where Voyager observations show considerable scatter, the observed values do vary only slowly with $r$, consistent with Equation (11.107). There is also good agreement among data from the three spacecraft despite their different positions in local time; only for $r \gtrsim 120\ R_J$ is there some indication of a significant systematic difference, Voyager 1 values tending to become higher than those from Voyager 2. For the distance range $40\ R_J \leq r \leq 80\ R_J$ (only for $r \leq 80\ R_J$ are all three spacecraft well inside the magnetosphere), Figure 11.11 shows $B_\circ/rB_r$, expressed as observed range within each 10 $R_J$ interval, as a function of local time; no significant local-time dependence is apparent.



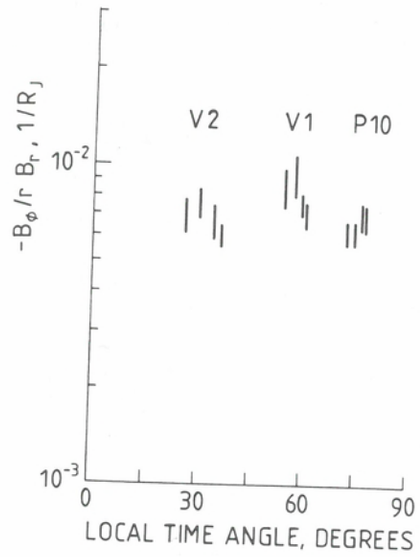


Fig. 11.11. The ratio $B_\circ/rB_r$ observed during the Pioneer 10, Voyager 1, and Voyager 2 outbound passes, as a function of local time angle measured from midnight. The bars represent the range that contains 50% of all observations within the radial distance intervals (from left to right for each pass) 40-50, 50-60, 60-70, and 70-80 $R_J$, taken from Figure 11.10 and from Figure 3 of Goertz et al. [1976]; the choice of 50% range eliminates extreme values associated with entry into or near the current sheet [from Vasyliunas, 1982*a*].

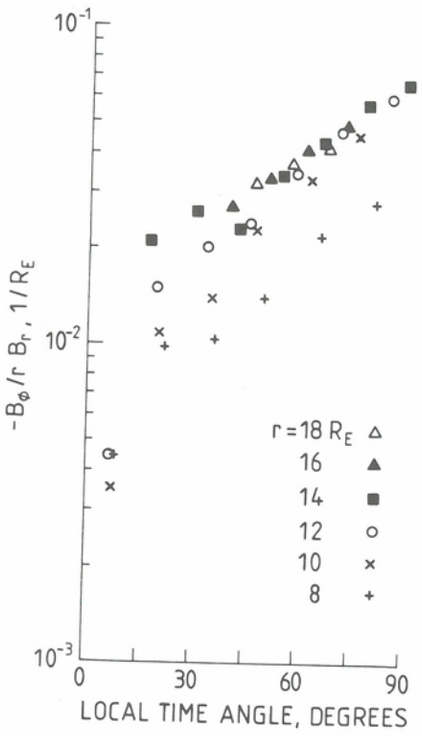


Fig. 11.12. The ratio $B_\circ/rB_r$ observed in the terrestrial magnetosphere as a function of local time, scaled from Figure 3 of Fairfield [1968] [from Vasyliunas, 1982a].

For comparison, Figure 11.12 shows $B_\circ/rB_r$ observed in the terrestrial magnetosphere [from Fairfield, 1968] as a function of local time in the midnight-to-dawn quadrant. In this case there is an obvious local-time variation, $B_\circ/rB_r$ decreasing toward midnight (as it should if it is to become zero there and to reverse sign on the dusk side); the

variation is present over a wide range of radial distances, including 12 to 18 $R_E$ where $B_\phi/rB_r$ is nearly independent of $r$. The fact that at Earth the magnetic field lines on the nightside are azimuthally bent by an amount that varies with local time, as expected from the action of a solar-wind-aligned magnetospheric tail, while at Jupiter the azimuthal bending of the field lines exhibits no corresponding variation and is essentially independent of local time (as expected from a rotation-related effect) within the observed regions of the nightside magnetosphere (except possibly in its very distant part, beyond 120 $R_J$) would seem to be a strong argument against assuming that all azimuthal fields in the magnetosphere arise from a common physical mechanism at both planets.

Local-time asymmetries do exist in the Jovian magnetosphere but they are observed primarily as day–night differences and not as variations within the midnight-to-dawn quadrant. On the dayside, the azimuthal magnetic field is generally smaller than on the nightside, although it still often exhibits a spiraling trend, evidenced by a qualitative tendency for $B_\phi$ and $B_r$ to have correlated magnitude variations and opposite signs [Jones, Thomas, and Melville, 1981]; a quantitative systematic radial variation analogous to Equation (11.107) has not been reported yet, however. A particularly weak and irregular $B_\phi$ was observed during the Pioneer 11 outbound pass, but whether this is a local time or a latitude effect – Pioneer 11 outbound went both closer to local noon and up to higher latitudes than any other spacecraft at Jupiter to date – is not yet entirely clear [see Smith, Davis, and Jones, 1976; Jones, Thomas, and Melville, 1981].

Modeling and theoretical studies of the azimuthal field have concentrated for the most part on the nightside magnetosphere, where Equation (11.107) may be applied and furthermore the usual assumption of axial symmetry has some direct observational support as noted previously. Among the topics of interest are the following: (1) relation of $B_\phi$ to the previously discussed models of the magnetic field, (2) global models of current systems associated with $B_\phi$, (3) quantitative models for spiraling of the magnetic field, (4) azimuthal stress balance and angular momentum transfer.

(1) With separation of the magnetic field into meridional and azimuthal components, $\mathbf{B} = \mathbf{B}_m + B_\phi \hat{\phi}$, and assumption of (at least local) axial symmetry, $(\partial/\partial\phi) = 0$, the Lorentz force density may be cast into the form

$$\mu_0 \mathbf{j} \times \mathbf{B} = (\nabla \times \mathbf{B}_m) \times \mathbf{B}_m - (1/2r^2) \nabla r^2 B_\phi^2 + \hat{\phi}\, (\mathbf{B}/r) \cdot \nabla r B_\phi \qquad (11.111)$$

A nonzero $B_\phi$ results in the appearance of an azimuthal stress component (third term) as well as modification of the magnetic stress in the meridional plane (second term). This modification, however, is slight as long as $B_\phi$ is relatively small compared to $|B_m|$. A model magnetic field calculated by neglecting $B_\phi$ will be changed, if $B_\phi$ is included, from $\mathbf{B}_m$ to $\mathbf{B}_m + \delta\mathbf{B}_m$ where

$$(\nabla \times \delta\mathbf{B}_m) \times (\mathbf{B}_m + \delta\mathbf{B}_m) + (\nabla \times \mathbf{B}_m) \times \delta\mathbf{B}_m = (1/2r^2) \nabla r^2 B_\phi^2 \qquad (11.112)$$

and it is apparent that, in order of magnitude,

$$\delta B_m / B_m \sim O(B_\phi^2/B_m^2) \sim O(r^2/r_J^2) \qquad (11.113)$$

where $r_J$ is defined in Equation (11.107). Hence, stress balance in the radial and vertical directions is little affected by the observed $B_\phi$ and most of the considerations and models of Sections 11.3.1, 11.3.2, and 11.3.3 remain applicable, until distances of the order of, or in excess of, some 80–100 $R_J$ are reached. Stress balance in the azimuthal direction is to be dealt with separately later.

(2) Associated with an azimuthal magnetic field there are in general electric current components in the radial and/or vertical directions, in addition to the azimuthal currents implied by the stretched-out configuration of the meridional magnetic field. The guiding principle in attempting to infer the large-scale current system associated with the observed $B_\phi$ is that strong currents perpendicular to $\mathbf{B}$ are possible only within the thin current sheet in the equatorial magnetosphere and within the Jovian ionosphere where the plasma stresses can be large enough to balance the $\mathbf{j} \times \mathbf{B}$ forces. Elsewhere, in the low-density region between the current sheet and the ionosphere, $\mathbf{j} \times \mathbf{B}$ must be very small and the magnetic field very nearly force-free, with currents flowing as Birkeland currents (i.e., along the magnetic field lines). Given these constraints, the qualitative configuration of the current system can be sketched immediately and is shown in Figure 11.13. The equatorial radial current density, integrated over (half) the thickness of the current sheet, is directly related to $B_\phi$ just outside the sheet,

$$\mu_0 j_r' = -B_\phi \qquad (11.114)$$

and can thus be inferred from observations. The various proposed models of the current system differ primarily in the assumed location of the Birkeland currents.



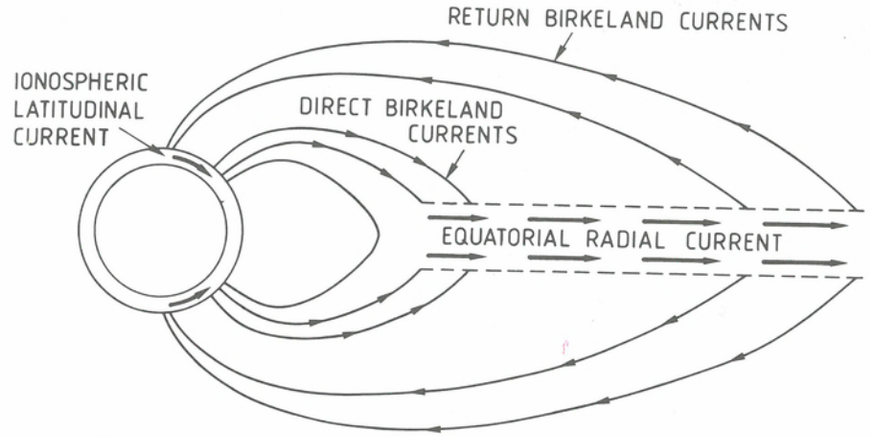


Fig. 11.13. Sketch of the current system associated with the azimuthal magnetic field, projected on a meridional surface. The size of Jupiter and the thickness of the ionosphere are greatly exaggerated for clarity [from Vasyliunas, 1982b].

Parish, Goertz, and Thomsen [1980] considered two alternative models, with the direct Birkeland currents either (1) distributed over the entire radial extent of the current sheet, with uniform current density $j_\parallel$ near the ionosphere, or (2) concentrated at the inner edge of the current sheet, assumed to lie at $r = 10\ R_J$; they compared both models with Pioneer 10 observations of $B_\phi$ and concluded that either model gave an adequate fit, within the observational uncertainties. Connerney [1981b; see also Thomsen and Goertz, 1981b] adopted their second model but gave a much simpler mathematical treatment and placed the inner edge with its Birkeland currents at $r = 5\ R_J$. The return Birkeland currents were emphasized by Connerney and mentioned by Parish, Goertz, and Thomsen (who placed them near the magnetopause) but not treated in detail in either paper.

With axial symmetry, the force-free assumption for the region above the current sheet implies, from Equation (11.111), that $rB_\phi$ is constant along a field line; with the help of Ampère's law it then follows that

$$r j_r' = R_J j_\theta' \sin\theta \qquad (11.115)$$

where $j_r'$ is the same as in Equation (11.114) and $j_\theta'$ is the height-integrated current in the ionosphere at the colatitude $\theta$ joined by a field line to the radial distance $r$ in the current sheet. The Birkeland current density $j_\parallel$ is given by current continuity together with Equation (11.114) as

$$\mu_0 j_\parallel B_z/B = (1/r)(\partial/\partial r)\, rB_\phi \tag{11.116}$$

just above the current sheet; within the force-free region $j_\parallel/B$ is constant along a field line. It is evident that if the Birkeland currents are concentrated at the inner and outer radial edges, $B_\phi$ above most of the current sheet must vary as $1/r$, as pointed out by Connerney [1981b], whereas distributed Birkeland currents imply a correspondingly different radial variation of $B_\phi$. (Note: the radial dependence of the ratio $j_r'/j_\phi'$ has no relevance to any of this, contrary to a remark by Jones, Melville, and Blake [1980].) Now Equation (11.107) with $F = 1$ and $B_r$ from the model of Goertz et al. yields $rB_\phi \sim r^{0.3}$, or a change between $r = 20\ R_J$ and $r = 80\ R_J$ by a factor 1.52 [reduced to 1.20 if $F$ given by Equation (11.110) is assumed]. Such changes hardly constitute a significant departure from constancy, given the uncertainties and fluctuations of the observed $B_\phi$ values; it is thus not surprising that it has not proved possible to extract from the available observations a unique model for the Birkeland current distribution.

If the dependence $rB_\phi \sim r^{0.3}$ is nevertheless taken at face value, Equation (11.116) implies, with $B_z$ from the model of Goertz et al.,

$$j_\parallel/B \sim r^{1.3}/[1 - (r/r_{nl})^{0.3}] \tag{11.117}$$

that is, $j_\parallel/B$ increases with increasing $r$, by a factor 8.7 if $C = 10$ or 16.8 if $C = 15$ between $r = 20\ R_J$ and $r = 80\ R_J$. By contrast, the two models of Parish, Goertz, and Thomsen assume $j_\parallel/B$ = constant and $j_\parallel/B \sim \delta(r - 10\ R_J)$, respectively, the second assumption implying $rB_\phi$ = constant. Widely different assumptions about the distribution of Birkeland currents can thus lead to rather similar radial profiles of $B_\phi$.

(3) The configuration of the azimuthal magnetic field described by Equation (11.107) is identical in form to the spiral pattern of magnetic field lines in interplanetary space, which results from the interaction of solar rotation with the radially outward solar wind flow [e.g., Parker, 1963; Hundhausen, 1972]. Hence, it has been widely assumed that $B_\phi$ within the nightside Jovian magnetosphere may be similarly attributed to the interaction of the planet's rotation with a radial outflow of magnetospheric plasma, such as the planetary/magnetospheric wind discussed in Section 11.4.3. The quantitative description of this interaction is based on the MHD relation between the electric field **E** and the plasma bulk flow velocity **V**:

$$\mathbf{E} + \mathbf{V} \times \mathbf{B} = 0 \tag{11.118}$$

With the use of * to designate quantities referred to a frame of reference rigidly corotating with Jupiter, Equation (11.118) may also be written as

$$\mathbf{E}^* + \mathbf{V}^* \times \mathbf{B} \equiv [\mathbf{E} + (\Omega_J \times \mathbf{r}) \times \mathbf{B}] + [\mathbf{V} - (\Omega_J \times \mathbf{r}) \times \mathbf{B} = 0 \tag{11.119}$$

Now if the ionospheric conductivity is sufficiently high, $\mathbf{E}^*$ becomes vanishingly small in regions of space connected to the ionosphere by magnetic field lines (see Sec. 11.4.2 for a more detailed argument) and Equation (11.119) then implies that $\mathbf{V}^*$ and **B** are aligned, whence in particular (in cylindrical coordinates)

$$B_\phi/B_r = (V_\phi - \Omega_J r)/V_r \tag{11.120}$$

and the further assumptions $V_\phi << \Omega_J r$, $V_r \sim$ constant yield an equation of the form



(11.107). To account for the observed spiraling of the field in the nightside Jovian magnetosphere, a value of the radial outflow speed

$$V_r \sim \Omega_J r_f = 2 \times 10^3 \text{ km/s}$$

is required at distances from about 20–40 $R_J$ to 100–120 $R_J$. This value is too large to be consistent with planetary wind theory, which predicts that the assumptions $V_\phi << \Omega_J r$ and $V_r \sim$ constant will hold only at distances where $V_r >> \Omega_J r$ (see Sec. 11.4.3). Furthermore, plasma observations do not indicate any strong radial outflow at distances smaller than 130–150 $R_J$ (Chaps. 3 and 4 and references therein). Thus a straightforward analogy with the Parker spiral in the solar wind does not provide an adequate model for $B_\phi$ in the Jovian magnetosphere.

An obvious weak point in the derivation of Equation (11.120) is the assumption that the Jovian ionospheric conductivity is sufficiently high to enforce corotation. As shown by Hill [1979] and discussed here in Section 11.4.4, plausible values of the ionospheric conductivity in fact allow large departures from corotational motion. Each constant-latitude strip of the ionosphere may then be characterized by the angular frequency $\Omega$ of its (longitude-averaged) actual azimuthal motion, with $\Omega \neq \Omega_J$ in general. This partial corotation will extend, by virtue of Equation (11.118), to the entire shell of magnetic field lines emanating from the fixed latitude, and the same derivation may be carried through as before to obtain Equation (11.120) but with $\Omega_J$ replaced by $\Omega$ everywhere. We then have

$$B_\phi/rB_r = (\omega - \Omega)/V_r \tag{11.121}$$

where $\omega \equiv V_\phi/r$ is the angular frequency of the azimuthal motion of plasma in the magnetosphere, to be distinguished both from $\Omega$ (which refers to the foot of the field line, in the ionosphere) and from $\Omega_J$. A latitudinal current in the ionosphere is driven by the electric field associated with the difference between $\Omega_J$ and $\Omega$:

$$j_\theta' = 2\Sigma B_J R_J (\Omega_J - \Omega) \sin\theta\, [(1 + 3\cos^2\theta)/4\cos\theta] \tag{11.122}$$

where $\Sigma$ is the height-integrated Pedersen conductivity of the ionosphere and the factor in brackets, which comes from the field inclination angle and its effect on the horizontal conductivity, may be set equal to one for all practical purposes (its value at a latitude as low as the $L = 6$ Io shell is 0.959). The ionospheric current is in turn related to the equatorial radial current and thence to $B_\phi$ by Equations (11.115) and (11.114), yielding

$$j_\theta' = -rB_\phi/\mu_0 R_J \sin\theta \tag{11.123}$$

Combining Equations (11.121), (11.122), and (11.123) and solving for $B_\phi$ and for $\Omega$ one obtains

$$B_\phi/rB_r = (\omega - \Omega_J)/[V_r + (1/\mu_0 \Sigma\chi)] \tag{11.124}$$

$$\Omega = \omega + (\Omega_J - \omega)V_r/[V_r + (1/\mu_0 \Sigma\chi)] \tag{11.125}$$

where

$$\chi \equiv 2B_J(R_J \sin\theta)^2/r^2 B_r \tag{11.126}$$

The foregoing derivation has been given by Vasyliunas [1982b].

The dimensionless quantity $\chi$, effectively a mapping factor between the equatorial plane and the ionosphere, depends only on the geometry of the magnetic field. From

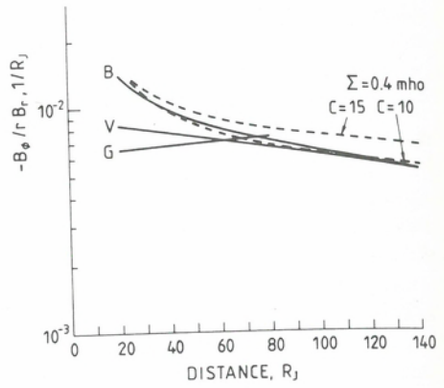


Fig. 11.14. Theoretical values of $B_\phi/rB_r$ (dashed lines) calculated from the theory described in the text with an assumed $\Sigma = 0.4$ mho and the field model of Goertz et al. [1976] with parameter $C = 10$ or 15, compared with various empirical fits (solid lines; see Fig. 11.10 for the nomenclature and note that the curve $B$ is not a good fit to the observations for $r < 40\ R_J$) [from Vasyliunas, 1982b].

equality of magnetic flux through corresponding segments of the ionosphere and the equatorial plane it can be shown that

$$B_J (R_J \sin\theta)^2 = M/r + \int_{R_J}^{r} r dr\, (B_{\text{dipole}} - B_z) \tag{11.127}$$

and thus $\chi$ can be evaluated from a field model that specifies $B_r$ and $B_z$ in the equatorial plane. Vasyliunas [1982*b*] calculated $\chi$ by using the model of Gleeson and Axford [1976] to carry out the integration in (11.127) from $r = 1\ R_J$ out to $r = 20\ R_J$ (in this range the model approximates well to the V 2 model of Connerney, Acuña, and Ness, see Fig. 11.8) and the model of Goertz et al. [1976] at larger distances; he found $\chi$ to be a slowly decreasing function of $r$, with values near 2 at $r = 25\ R_J$ and near 1 at $r = 100\ R_J$.

Two limiting cases are of interest. In the high-conductivity limit,

$$\mu_0 \Sigma \chi V_r = \chi(\Sigma/1\ \text{mho})\,(V_r/796\ \text{km s}^{-1}) >> 1 \tag{11.128}$$

Equation (11.124) reduces to (11.120) and (11.125) reduces to $\Omega = \Omega_J$; we recover the expected full corotation of the ionosphere and the Parker spiral for the magnetic field. More relevant to the Jovian magnetosphere is the opposite, low-conductivity limit. With the inequality in (11.128) reversed, Equations (11.124)–(11.125) reduce to

$$B_\phi/rB_r = (\omega - \Omega_J)\,\mu_0 \Sigma \chi \tag{11.129}$$

$$\Omega = \omega \tag{11.130}$$

The ionosphere now corotates with the magnetospheric plasma but not necessarily with the planet (the value of $\omega$, governed by azimuthal stress balance, is not determined by the model in any limit); the spiraling angle of the magnetic field is now proportional to the ionospheric conductivity and does not depend on $V_r$.

Numerical values of $B_\phi/rB_r$ predicted by Equation (11.129) for the case $\omega << \Omega_J$, with $\Sigma = 0.4$ mho and $\chi$ calculated as described previously, are shown in Figure 11.14 together with the several fits to observed values (see Fig. 11.10 and associated discussion). The agreement between theory and observation is quite good (except at close distances, where the assumption $\omega << \Omega_J$ may not hold) for the model with $C = 10$ with the chosen conductivity; an equally good agreement for the model with $C = 15$ can be obtained by choosing $\Sigma = 0.33$ mho. These conductivity estimates are to be regarded as lower limits; if either $\omega$ or $V_r$ are nonnegligible, higher values of $\Sigma$ are required to maintain the fit to the observations. ($V_r$ is insignificant unless it approaches or exceeds $10^3$ km/s.)



The observed azimuthal magnetic fields in the nightside Jovian magnetosphere can thus be quantitatively accounted for as a simple consequence of finite ionospheric conductivity and partial corotation, without the necessity of postulating unrealistically large radial outflow speeds. In simplest physical terms, the model states that the ionospheric continuation of the equatorial radial current associated with $B_\phi$ (see Fig. 11.13) is simply the current driven by the meridional electric field that is applied to the conducting ionosphere as a result of partial corotation. There is a maximum possible value of this electric field, corresponding to near-zero corotational motion ($\Omega \to 0$); thus from observations of $B_\phi$, which together with a magnetic field model for the mapping factor $\chi$ determine a definite amount of current to be driven through the ionosphere, a minimum required ionospheric conductivity of some 0.3–0.4 mho can be inferred.

(4) The azimuthal component of the tangential stress balance Equation (11.18), can be written in the form

$$\sigma(d/dt)\omega r^2 = 2rB_\phi B_z/\mu_0 \tag{11.131}$$

where

$$(d/dt) \equiv \partial/\partial t + V_r \partial/\partial r + \omega\, \partial/\partial\phi \tag{11.132}$$

and $2B_\phi$ is the (vector) difference of the oppositely directed azimuthal field components above and below the current sheet. The pressure gradient term has been neglected, both on the general grounds discussed in Section 11.2.2 and because $\partial P/\partial\phi$ is likely to be small in any case and vanishes for axial symmetry. Equation (11.131) states that the torque exerted by the azimuthal magnetic field acts to change the angular momentum of the plasma. It is convenient to introduce the quantity

$$S \equiv r \int d\phi\, \sigma V_r \tag{11.133}$$

(with the integration carried out over an angular sector of width $\Delta\phi$) which represents the integrated net mass flux across the cylinder (or cylinder segment if $\Delta\phi \neq 2\pi$) at a radial distance $r$. If $\partial/\partial t$ and $\partial/\partial\phi$ in (11.132) are either assumed negligible or averaged over, Equation (11.131) may be integrated to give

$$S(d/dr)\,\langle\omega\rangle\, r^2 = 2r^2 \int d\phi\, B_\phi B_z/\mu_0 = 2r^2 B_\phi B_z\, \Delta\phi/\mu_0 \tag{11.134}$$

where the second form assumes axial symmetry of the magnetic field. The average local rotation frequency $\langle\omega\rangle$ is defined by

$$\langle\omega\rangle \equiv r \int d\phi\, \sigma V_r\, \omega/S \tag{11.135}$$

If, furthermore, inflow of plasma into the current sheet from above and below (e.g., from an ionospheric source) is neglected, then, by conservation of mass, $S$ is independent of $r$ (except within the Io torus or other plasma source regions).

Note that $\langle\omega\rangle$ is an average weighted by the radial mass flux $\sigma V_r$. If the outward mass transport occurs predominantly by simple radial outflow so that $\sigma V_r > 0$ at all $\phi$, then $\langle\omega\rangle$ approximates to a straightforward average over $\phi$. In this case the observed fact that $B_\phi$ has the same sign at all $r$ implies, together with Equation (11.129), that $\langle\omega\rangle \leq \Omega_J$; that is, there can be on the average no supercorotation of the plasma as that would imply an opposite sense of $B_\phi$ to what is observed. The angular momentum added to the plasma by the magnetic torque is in this case transported outward by simple advection, the flowing plasma carrying angular momentum with it. If, on the other hand, the predominant plasma motion is one of circulation, radial flow occurring both inward and outward and a net outward mass transport resulting only from a larger mass flux in the outflow regions compared to the inflow (as in models of corotating

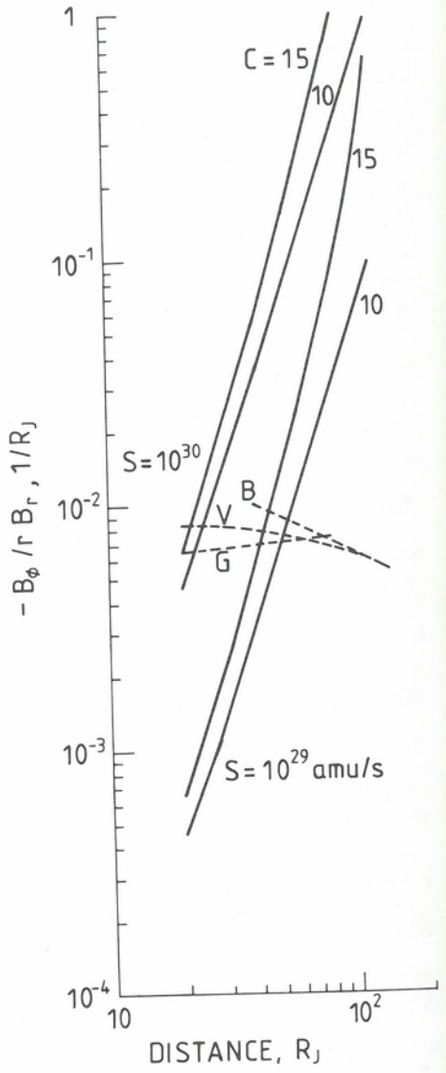


Fig. 11.15. The value of $B_\phi/rB_r$ needed to maintain full corotation of the plasma for various values of the mass flux $S$ (solid lines), calculated with use of the Goertz et al. [1976] model with the two values of $C$, and the various empirical fits (dashed lines, see Fig. 11.10).

convection or of radial diffusion, described in Sections 11.4.6 and 11.4.7), then $\langle\omega\rangle$ may be written as

$$\langle\omega\rangle = (S_{out}\,\omega_{out} - S_{in}\,\omega_{in}) / (S_{out} - S_{in}) \tag{11.136}$$

where $S_{out}$ is the mass flux integrated over the part of the cylindrical surface where $\rho V_r > 0$, $\omega_{out}$ the associated average $\omega$, and $S_{in}$ with $\omega_{in}$ defined similarly where $\rho V_r < 0$; since $S \equiv S_{out} - S_{in}$, (11.136) may be rewritten as

$$\langle\omega\rangle = \omega_{out} + (S_{in}/S)\,(\omega_{out} - \omega_{in}) \tag{11.137}$$

It is thus possible now for $\langle\omega\rangle$ to become much larger than $\Omega_J$, even when $\omega_{out} \leq \Omega_J$ and $\omega_{in} \leq \Omega_J$, provided $S_{in}/S$ is sufficiently larger than one, that is, the net outward mass flux is much smaller than the total mass flux in the circulating motion. In this case the



angular momentum can be transported outward by means of an effective eddy viscosity: outflowing plasma carries more angular momentum than inflowing plasma ($\omega_{out} > \omega_{in}$) with the result of a net outward angular momentum flux even if the net outward mass flux is small or negligible (hence $\langle\omega\rangle$, defined as the ratio of the two fluxes, is allowed to become very large).

Given the (constant) value of $S$, Equation (11.134) constitutes a relation between $\langle\omega\rangle$ and $B_\phi$, from which either can be calculated given the other. In the following calculations we take $\Delta\phi = 90°$, corresponding to the midnight-to-dawn quadrant, approximately within which a well-defined, nearly axially symmetric structure of $B_\phi$ has been observed; values of $S$ refer then to this quandrant, but they can be easily scaled for other assumptions, for example, doubled if outflow over the entire 180° of the nightside is assumed. Values of $B_z$ (and of $B_r$ where needed) are taken from the model of Goertz et al. [1976].

Setting $\langle\omega\rangle = \Omega_J$ in Equation (11.134) determines the $B_\phi$ needed to maintain the plasma within the current sheet in rigid corotation; the calculated $B_\phi$ scales in proportion to $S$ and is shown in Figure 11.15 for two values of $S$ (actually the quantity $B_\phi/rB_r$ is plotted, for convenience in comparison with the observations). In contrast to the nearly constant observed values, $B_\phi/rB_r$ required to maintain rigid corotation increases sharply with increasing $r$, a consequence of the fact that the angular momentum per unit mass of rigidly corotating plasma increases as $r^2$ and hence must be supplied, if the plasma is transported outward from a source in the inner magnetosphere, by an ever-increasing magnetic torque. It is also apparent from the figure that if $S = 10^{30}$ amu/s, generally considered a reasonable estimate (see Chap. 10 and references therein), then the observed $B_\phi$ is far too small to enforce corotation at distances beyond about 20–25 $R_J$. If $S = 10^{29}$ amu/s, the observed $B_\phi$ is at first far larger than what is needed but then also becomes too small at distances beyond about 45–55 $R_J$.

It is also possible to set $B_\phi$ in Equation (11.134) equal to the observed values and, by integrating the equation, to obtain the implied $\langle\omega\rangle$ as a function of $r$. The result may be written as

$$\langle\omega\rangle = (T/r^2\,S) + \omega_1\,(r_1/r)^2 \tag{11.138}$$

where

$$T = 2\Delta\phi \int_{r_1}^{r} dr'(r')^2\,B_\phi\,B_z/\mu_0 \tag{11.139}$$

is the integrated magnetic torque on a segment of the current sheet from $r_1$ to $r$ and $\omega_1$ is the boundary value of $\langle\omega\rangle$ at $r = r_1$. Numerical results for $\omega_1 = \Omega_J$ at $r_1 = 20\ R_J$, with $B_\phi$ taken from Equation (11.107) with $F = 1$, are shown in Figure 11.16*a* for various values of $S$. Consistent with Figure 11.15 and associated discussion, for $S = 10^{31}$ amu/s $\langle\omega\rangle$ decreases sharply with increasing $r$ and is not much above the $\omega_1\,(r_1/r)^2$ value for negligible magnetic torque per unit mass ($S \to \infty$), while for $S = 10^{29}$ amu/s the initially large magnetic torque raises $\langle\omega\rangle$ to values much above $\Omega_J$, with an increase of angular momentum that then suffices to maintain $\langle\omega\rangle > \Omega_J$ even to $r = 100\ R_J$ where $B_\phi$ has become much smaller. For $S = 10^{30}$ amu/s, with the observed $B_\phi$ somewhat above the corotational value just for a short interval beyond 20 $R_J$, $\langle\omega\rangle$ initially rises slightly above $\Omega_J$ and then decreases sharply. (The critical value of $S$, above which there is no initial rise above $\Omega_J$ at $r_1 = 20\ R_J$, can be shown to be $S = 4.0 \times 10^{30}$ amu/s for the $C = 10$ model and $S = 2.8 \times 10^{30}$ amu/s for $C = 15$.) Similar results are obtained if the plasma is assumed to be only partially corotating at $r_1 = 20\ R_J$ already, as shown in Figure 11.16*b* for $\omega_1 = 0.5\ \Omega_J$.

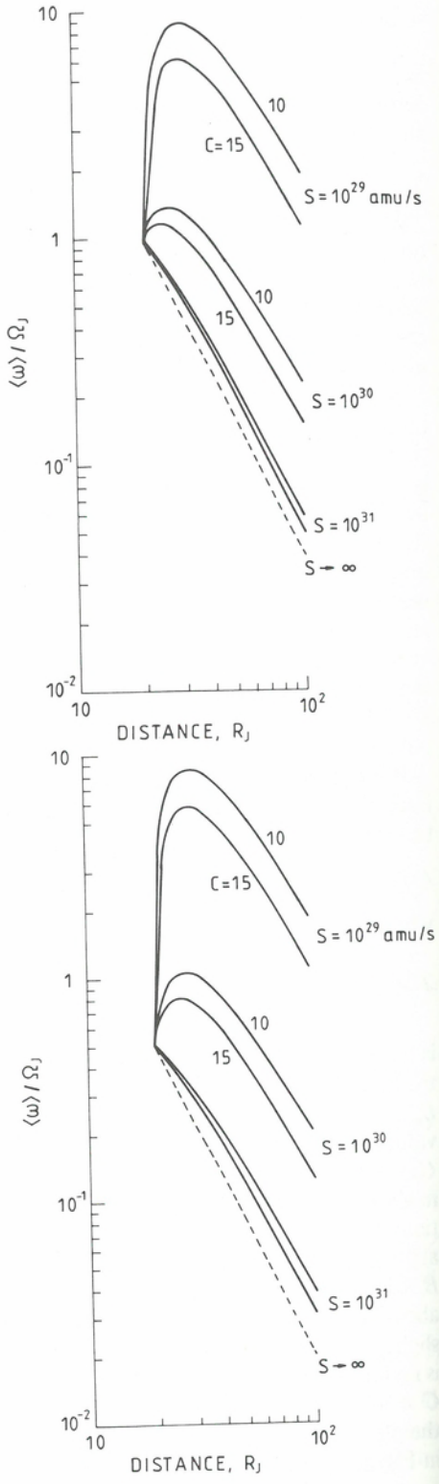


Fig. 11.16. (*a*) Average angular speed of the plasma calculated from an empirical fit to the observed $B_\phi$ and the two versions of the Goertz et al. [1976] model, with assumed full corotation at $r = 20\ R_J$, for various values of the mass flux $S$. (*b*) The same but with $\omega = 0.5\ \Omega_J$ at $r = 20\ R_J$ assumed as the boundary condition.



As mentioned previously, values of $\langle\omega\rangle > \Omega_J$ are acceptable only if $S << S_{in}$; otherwise, in a simple radial outflow, $B_\phi$ would decrease to zero as $\omega \to \Omega_J$ and thus no angular acceleration to $\omega > \Omega_J$ could occur. The following conclusion can therefore be drawn: if the net mass outflow rate $S$ is less than about $10^{30}$ amu/s, the angular momentum must be transported outward by means of an effective eddy viscosity mechanism and an amount of mass much larger than $S$ must be circulating in and out through the outer magnetosphere; if, on the other hand, the angular momentum is simply advected by the outward-flowing plasma, $S$ must be significantly larger than $10^{30}$ amu/s. In any case, a mass flow of something like $10^{30}$–$10^{31}$ amu/s from the inner to the outer magnetosphere seems to be almost unavoidable, given the torques implied by the observed azimuthal magnetic field, and the only question is whether a major fraction of this mass returns to the inner magnetosphere (forming a vast circulation/convection system) or whether most of it flows out of the magnetosphere (in the form of a planetary/magnetospheric wind).

The total magnetic torque implied by the observed $B_\phi$ or equivalently the angular momentum flux in the magnetic field can of course be calculated independently of any assumptions about the mass flux. The magnetic torque on the current sheet integrated from $r = 20$ to $100\ R_J$ over a $\Delta\phi = 90°$ segment is, from evaluation of Equation (11.139),

$$T_{cs} = 1.4 \times 10^{18}\ \text{Nm (if } C = 10) \qquad (11.140)$$
$$= 8.1 \times 10^{17}\ \text{Nm (if } C = 15)$$

This is the angular momentum per unit time transferred from the magnetic field to the plasma within the current sheet. In addition, the magnetic field above and below the current sheet at $r = 100\ R_J$ implies a magnetic angular momentum flux, through a cylindrical surface, given by

$$T_B = 2r^3 \sin\theta\, \Delta\phi\, B_r\, B_\phi/\mu_0 = 2.4 \times 10^{18}\ \text{Nm} \qquad (11.141)$$

where the latitudinal extent $\theta$ of the region with $B_\phi$ equal to the observed values has been set to 9.6° (the dipole tilt angle, roughly equal to the maximum magnetic latitude sampled by Pioneer 10 outbound) and $\Delta\phi = 90°$ again; this represents a torque exerted on plasma lying beyond $100\ R_J$. For comparison, the angular momentum flux associated with a mass flux $S$ corotating at $r = 20\ R_J$ is

$$T_m = S\,\Omega_J\, r^2 = (S/10^{30}\ \text{amu/s})\ 6.0 \times 10^{17}\ \text{Nm} \qquad (11.142)$$

which presumably equals the total magnetic torque at distances $r < 20\ R_J$ that acts to maintain the plasma in corotation.

All three quantities – $T_{CS}$, $T_B$, and $T_m$ – also represent torques acting against the rotation of Jupiter and extracting energy from it, at a rate given by $\Omega_J$ times torque. The implied power is, for each of the three torques,

$$P_{CS} = 4.9 \times 10^{14}\ \text{W (if } C = 10) \qquad (11.143)$$
$$= 2.9 \times 10^{14}\ \text{W (if } C = 15)$$
$$P_B \approx 8.5 \times 10^{14}\ \text{W}$$
$$P_m = (S/10^{30}\ \text{amu/s})\ 1.1 \times 10^{14}\ \text{W}$$

(For the estimates of $P_{CS}$ and $P_B$, the torques given by (11.140) and (11.141) were multiplied by a factor of 2, to allow for an equal contribution from the dusk–midnight quadrant.) These numbers represent the total power supplied by loss of rotational energy.

Not all of it, however, may be available for "interesting" phenomena like particle energization or auroral radiation. Dessler [1980b] and Eviatar and Siscoe [1980] have pointed out that one half of $P_m$ is required to supply the corotational kinetic energy of the outflowing plasma. Joule dissipation in the ionosphere also claims a share of the total power. By noting that the torque can be calculated from the Lorentz force on the ionospheric current $j_\theta'$ given by Equation (11.122) while the Joule dissipation is obtained from $(j_\theta')^2/\Sigma$, it is readily shown that a rough estimate for the fraction of the total power that must go into Joule dissipation is $(\Omega_J - \Omega)/\Omega_J$; hence if $\Omega \approx \omega << \Omega_J$ in the outer magnetosphere, much if not most of $P_{CS}$ and $P_B$ may be expended in Joule heating of the ionosphere.

The foregoing discussion has taken for granted the fundamentally rotational origin of azimuthal magnetic fields in the Jovian magnetosphere and hence the expected similarity of dawn and dusk sides, with the same sign of $B_\infty$ (for this reason the magnetic torques were doubled to obtain the power). If instead a solar-wind-aligned magnetospheric tail origin is assumed, so that the dawn and dusk sides are again similar but with reversed signs of $B_\infty$, then the magnetic torques from the two sides cancel and $P_{CS}$ and $P_B$ vanish; $P_m$ remains as the sole power supplied by the planetary rotation. The discussion given of magnetic field spiraling and azimuthal stress balance would remain, on the whole, valid but applicable to the dawnside only. On the duskside, a similar discussion but with reversed $B_\infty$ presents many problems that have hardly been considered yet by either the proponents or the opponents of the solar wind interpretation. Fundamentally, the spiraling and the azimuthal stress are opposed: on the dawnside, as we have seen, the spiraling requires that the plasma lag behind rigid corotation, while the azimuthal magnetic stress tends to bring it back to corotation, and a sufficiently large rate of mass through-flow is needed to prevent the magnetic stress from destroying the spiraling (and itself with it). A nonmagnetic stress opposed to corotation, required to set up the plasma lag in the first place, is provided by the inertia of outflowing plasma (and could in principle also be provided by solar wind drag, as originally suggested by Piddington). If now $B_\infty$ on the duskside is reversed in sign, the spiraling will require that the plasma rotate faster than rigid corotation, in opposition to the azimuthal magnetic stress, again demanding a sufficiently large rate of mass through-flow to maintain the configuration and a nonmagnetic stress in the direction of corotation to set it up. Such a nonmagnetic stress could be provided by the inertia of *inflowing* plasma (with sufficient initial angular momentum), as discussed recently in another context by Hill, Goertz, and Thomsen [1982]; solar wind drag would be effective for this purpose only if the flow speed of solar wind plasma near the magnetopause exceeds the speed of corotation.

### 5. Dipole tilt and solar wind effects

When the relatively small but nonzero tilt angle $\alpha \approx 9.6°$ between Jupiter's rotation axis and its magnetic dipole moment is no longer neglected, it becomes necessary to consider explicitly where the current sheet is located because now there is no plane perpendicular to both the rotation axis and the dipole moment. The momentum Equation (11.1) resolved into components normal and tangential to the current sheet at a given point may be written

$$\hat{\mathbf{n}}\,[\rho(d\mathbf{V}/dt)\cdot\hat{\mathbf{n}} + (\partial/\partial n)\,(P + B_p^2/2\mu_0)] = \hat{\mathbf{n}}\,\hat{\mathbf{n}}\cdot\mathbf{j}_t\times(\mathbf{B} - \mathbf{B}_p) \tag{11.144}$$

$$\rho(d\mathbf{V}/dt)_t + \nabla_t P = \mathbf{j}_t\times\hat{\mathbf{n}}\,(\mathbf{B} - \mathbf{B}_p)\cdot\hat{\mathbf{n}} \tag{11.145}$$



(for the definition of $\mathbf{B}_p$, see Equation (11.10) and associated discussion). Equation (11.144) is obtained from (11.11) and (11.21) (the symbol $\hat{\mathbf{z}}$ has been replaced by $\hat{\mathbf{n}}$ to emphasize that we are dealing with directions normal and tangential to the actual current sheet and not with an independently prescribed coordinate system); pressure anisotropy and the small normal component of $\mathbf{j}$ (given by $\nabla_t\times\mathbf{B}_t$) have been neglected. These equations imply that $\mathbf{B} - \mathbf{B}_p$ is perpendicular to the vector formed by their LH sides. We now define the center of the current sheet as the point where $P + B_p^2/2\mu_0$ reaches its maximum value and hence $(\partial/\partial n)\,(P + B_p^2/2\mu_0) = 0$. It follows that

$$(\mathbf{B} - \mathbf{B}_p)\cdot(\rho\, d\mathbf{V}/dt + \nabla_t P) = 0 \tag{11.146}$$

at the center of the current sheet. An equivalent result involving quantities integrated across the thickness of the current sheet can be derived by noting that the integral of $(\partial/\partial n)\,(P + B_p^2/2\mu_0)$ yields zero because $B_p^2$ by definition has the same value on both sides of the current sheet and $P$ is negligibly small outside it.

Equation (11.146) or its integral counterpart serves to determine the location of the current sheet. It states that the external magnetic field at the current sheet (i.e., the field minus the local planar field of the current sheet itself) must be perpendicular to the vector formed by the inertial stress plus the tangential part of the pressure gradient – the normal pressure gradient and the Lorentz force of the planar field balance each other. In the cold-plasma limit, with $\nabla_t P$ negligible in comparison to the inertial term, $\mathbf{B} - \mathbf{B}_p$ must be perpendicular to the plasma acceleration. In particular, with corotating plasma and $\mathbf{B} - \mathbf{B}_p$ approximated by the dipole field $\mathbf{B}_d$, the center of the current sheet lies in the surface defined by

$$\mathbf{B}_d\cdot(\mathbf{r} - \hat{\Omega}\,\hat{\Omega}\cdot\mathbf{r}) = 0 \tag{11.147}$$

that is, the locus of points where each field line reaches its maximum distance from the rotation axis, a result familiar in the literature [e.g., Gledhill, 1967; Hill, Dessler, and Michel, 1974]. This surface, known as the centrifugal symmetry surface or the centrifugal equator, is easily shown to be given by the equation (in cylindrical coordinates about the *rotation* axis)

$$z/r\cos\phi = -(4/3)\tan\alpha/\{1 + [1 + (8/9)\cos^2\phi\tan^2\alpha]^{1/2}\} \tag{11.148}$$

where $\phi$ is the longitude angle measured from the prime meridian plane containing $\hat{\Omega}$ and the dipole moment $\mathbf{M}$ (assumed tilted by an angle $\alpha$ toward the positive $x$ axis). Because of the factor $\cos^2\phi$ in the denominator, this surface is not exactly a plane (contrary to a statement by Hill, Dessler, and Michel) but the deviations from planarity amount to no more than a fractional change in $z/x$ by a factor $\leq 1 + (2/9)\tan^2\alpha = 1.006$, far smaller than the neglected effects of nondipolar field components or of gravitational acceleration. The surface lies between the rotational and the magnetic equator and forms an angle $\beta$ with the magnetic equator given by $\tan(\beta - \alpha) =$ RH side of (11.148) with $\cos\phi = \pm 1$, which can be shown to yield

$$\tan\beta = (2/3)\tan\alpha/\{1 + [1 + (8/9)\tan^2\alpha]^{1/2}\} \tag{11.149}$$

a formula given by Hill, Dessler, and Michel. With $\alpha = 9.6°$, Equation (11.149) gives $\beta = 3.2°$.

In the opposite limit of a hot plasma, with the pressure gradient dominant over the inertial term, $\mathbf{B} - \mathbf{B}_p$ must be perpendicular to $\nabla_t P$ and hence normal to the current sheet; if $\mathbf{B} - \mathbf{B}_p \approx \mathbf{B}_d$ the current sheet lies in the magnetic equator. In the general case, then, the center of the current sheet, defined as above by the maximum of

$P + B_p^2/2\mu_0$, is expected to lie between the magnetic equator and the centrifugal symmetry surface, approaching the one or the other as the ratio of thermal to corotational speed becomes large or small. At the same time, the maximum of the plasma pressure $P$ alone always occurs at the centrifugal symmetry surface, for any value of the temperature, as shown in Section 11.2, Equation (11.47). It is thus obvious that, with a nonnegligible dipole tilt, the current sheet is necessarily asymmetric about its center and its width is large enough to encompass the centrifugal symmetry surface, reaching a value $h \gtrsim r \tan \beta$ in the hot-plasma limit.

Quantitative modeling of the current sheet location on the basis of Equation (11.146) with neither term neglected has so far proved feasible only in the prime meridian plane, where, by symmetry, $\nabla_t P$ is coplanar with $d\mathbf{V}/dt$. The following description is based on the approach of Goertz [1976b], with some corrections and generalizations. Let $r$, $z$ be cylindrical coordinates with respect to the *dipole* axis, so that in the prime meridian

$$\hat{\Omega} = -\hat{\mathbf{r}} \sin \alpha + \hat{\mathbf{z}} \cos \alpha \tag{11.150}$$

Let $z = Z(r)$ be the location of the center of the current sheet; then the direction normal to the current sheet is

$$\hat{\mathbf{n}} = [\hat{\mathbf{r}}(dZ/dr) + \hat{\mathbf{z}}] / [1 + (dZ/dr)^2]^{1/2} \tag{11.151}$$

It may be assumed that $\alpha << 1$, $|Z/r| << 1$, and $|dZ/dr| << 1$, with the calculation carried out to lowest order in these quantities. With this approximation, the components of the centripetal acceleration and of the dipole field normal and tangential to the current sheet, evaluated at its center, are

$$(d\mathbf{V}/dt) \cdot \hat{\mathbf{n}} = -\Omega_J^2 r [\sin \alpha + dZ/dr] \tag{11.152}$$

$$(dV/dt) \cdot \hat{\mathbf{t}} = -\Omega_J^2 r$$

$$\mathbf{B}_d \cdot \hat{\mathbf{t}} = -M/r^3$$

$$\mathbf{B}_d \cdot \hat{\mathbf{t}} = (M/r^3)[3Z/r + dZ/dr]$$

(Note: Goertz [1976b] mistakenly omits the terms $dZ/dr$, resolving his vectors along $\hat{\mathbf{z}}$, $\hat{\mathbf{r}}$ rather than $\hat{\mathbf{n}}$, $\hat{\mathbf{t}}$.) Furthermore, we set

$$\mathbf{B} - \mathbf{B}_p = \mathbf{B}_d + b_n \hat{\mathbf{n}} + b_t \hat{\mathbf{t}} \tag{11.153}$$

where $\mathbf{b}$ represents any external fields other than the planetary dipole, and parameterize the pressure gradient by the expressions (11.26) and (11.100). Inserting these together with (11.152) and (11.153) into (11.146) and rearranging yields a differential equation for $Z(r)$

$$[1 + (\mu r^3 b_n/M)]\, dZ/dr + 3(1 + \mu)\, Z/r - [1 - (r^3 b_n/M)]\, \mu \sin \alpha - (1 + \mu)\, r^3 b_t/M = 0 \tag{11.154}$$

to be solved with the boundary condition $Z \to 0$ as $r \to 0$.

Assume first that $b_n = b_t = 0$, that is, only the dipole field is present in addition to the planar field of the current sheet itself. The solution of Equation (11.154) for any specified radial dependence of $\mu$ is given by

$$g(r)\, Z(r) = \sin \alpha \int dr\, g(r')\, \mu(r') \tag{11.155}$$

where

$$g(r) \equiv \exp \{3 \int [1 + \mu(r)]\, dr/r\} \tag{11.156}$$



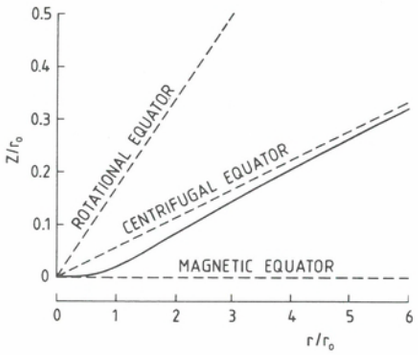


Fig. 11.17. Calculated variation of current sheet position with the assumption $\mu \sim r^2$. The distance $r_0$ is defined by $\mu = 1$, pressure gradient equals centrifugal force density. Note the difference in horizontal and vertical scales.

If $\mu$ is independent of $r$ (the thermal speed increases in proportion to the corotational speed),

$$Z = r \sin \alpha / [3 + (4/\mu)] \tag{11.157}$$

a straight line whose slope varies from zero (current sheet in the magnetic equator) in the hot-plasma limit $\mu = 0$ to (1/3) sin $\alpha$ (current sheet in the centrifugal symmetry surface, with $\sin \alpha \approx \tan \alpha$ within the approximations used) in the cold-plasma limit $\mu \to \infty$, as expected from the previous qualitative discussion; when $\mu = 1$, that is, the pressure gradient and the centrifugal force density are equal, $Z/r = (1/7) \sin \alpha$ and the current sheet is approximately half way between the two limits. If the thermal speed is independent of $r$ so that $\mu$ varies as $r^2$, the solution is

$$(3/2)^{1/2} Z = (r_0/3) \sin \alpha \{s^4 - 2s^2 + 2[1 - \exp(-s^2)]\}/s^3 \tag{11.158}$$

where $s \equiv (3/2)^{1/2} r/r_0$ and $r_0$ is the distance at which $\mu = 1$; for small and large values of $r$,

$$Z = (r_0/6) \sin \alpha\, (r/r_0)^3 [1 - (3/2)(r/r_0)^2 + \ldots] \qquad r << r_0 \tag{11.159}$$

$$Z = (r/3) \sin \alpha [1 - (4/3)(r_0/r)^2 + \ldots] \qquad r >> r_0$$

and the complete solution is shown in Figure 11.17. The current sheet in this case is appreciably curved, and the expected transition, from the magnetic equator at $r << r_0$, where the corotational speed is small compared to the thermal speed, toward the centrifugal equator at $r >> r_0$ where the corotational speed is large, is clearly apparent.

When $\mathbf{b}$ is not neglected, the solution is a straight line if and only if the quantities $\mu$, $r^3 b_n$ and $r^3 b_t$ are all independent of $r$. Goertz [1976b] set $r^3 b_n/M$ to the constant value implied by his field model with variable current sheet thickness (see Sec. 11.3.3) and given here by Equation (11.106); he further implicitly assumed that $b_t = 0$ and $\mu =$ constant. With these assumptions, the solution of Equation (11.154) is

$$Z = r \sin \alpha / [3 + (4/\mu) + 4a\, C/\mu\, (1 + a)] \tag{11.160}$$

or in terms of the parameter $k \equiv 1/\mu\, (1 + a)$ used by Goertz

$$Z = r \sin \alpha / [3 + 4k(1 + a + aC)] \tag{11.160'}$$

(the corresponding equation of Goertz has a coefficient $3k$ instead of $4k$, a result of his neglecting $dZ/dr$). As the hot-plasma limit is approached, $Z$ now decreases toward the magnetic equator $Z = 0$ much more rapidly than in the case when $b_n = 0$, because of the added term proportional to $aC$ in the denominator. However, the validity of this

result may be questionable because it depends on the assumption $b_t = 0$ and even relatively small values of $b_t$ (such as may be expected from the previously noted necessary asymmetry of the current sheet, whose center defined by the condition $\partial/\partial n$ $(P + B^2/2\mu_0) = 0$ need not coincide with the surface defined by either $\mathbf{B}_t = 0$ or $\mathbf{B}_p = 0$) may have a significant effect; as a simple example, if we set $b_t = \epsilon b_n \sin\alpha$ ($b_t = 0$ of course when $\alpha = 0$), Equation (11.160′) is replaced by

$$Z = r\sin\alpha\,[1 + \epsilon kaC]\,/\,[3 + 4k(1 + a + aC)] \tag{11.161}$$

so that a term proportional to $aC$ now appears in the numerator as well.

By definition, **b** includes magnetic fields from all sources other than the planetary dipole and the local sheet current. In general, the direction of **b** has no simple relation to the local normal to the current sheet; thus $b_n$ and $b_t$ may depend linearly on $dZ/dr$, with a consequent change in the coefficients of the differential Equation (11.154). It has been suggested [Hill, Dessler, and Michel, 1974; Smith et al., 1974a] that at large distances the current sheet should bend away from the centrifugal symmetry surface and become parallel to the rotational equator. Setting **b** equal to the magnetic field of the entire current sheet minus the field of the local sheet current (the "curvature" field as distinct from the "planar" field, in the terminology of Mead and Beard [1964]) should provide a quantitative description of such an effect, but no specific models have yet been developed.

The geometrical configuration of the current sheet is expected to be stationary in the rigidly corotating frame of reference where the planetary dipole is fixed (except in the outermost regions of the magnetosphere where local-time variations are significant). It has been tacitly assumed throughout the foregoing discussion that the plasma is effectively at rest in this corotating frame. When the plasma motion deviates significantly from rigid corotation, the plasma becomes subject to vertical accelerations as the tilted and possibly curved current sheet configuration rotates with respect to it. The term $(d\mathbf{V}/dt) \cdot \hat{\mathbf{n}}$ in Equation (11.144) is then no longer equal to the centripetal acceleration and in general cannot be specified a priori. It becomes more appropriate to view Equation (11.144) as a statement that an imbalance of applied normal stresses determines the instantaneous vertical acceleration of the current sheet and hence the time history of its location. In effect, the current sheet now becomes a wave, generated by a rotating tilted dipole and propagating radially outward. Discussions of the current sheet from this point of view (mostly qualitative or based on simple analogies to Alfvén waves) have been given by, among others, Northrop, Goertz, and Thomsen [1974], Prakash and Brice [1975], Eviatar and Ershkovich [1976], Kivelson et al. [1978], Carbary [1979], and Goertz [1981]. The various empirical representations of the current sheet and their relation to these as well as to alternate models are reviewed in Chapters 1, 5, and 10. A longitude-averaged effective radial propagation speed for the shape of the current sheet of 40–45 $R_J$/hr, independent of radial distance, provides a good fit to the Pioneer 10 outbound observations [Kivelson et al., 1978] as well as to Voyager 1 and 2 [Bridge et al., 1976b; Carbary, 1979; Goertz, 1981; Vasyliunas and Dessler, 1981].

The extent of solar-wind influence on the magnetic field configuration within the Jovian magnetosphere is a matter of considerable controversy, some aspects of which have already been discussed in Section 11.3.4 as well as in Chapters 1 and 10. Sufficiently far downstream of Jupiter, a magnetotail analogous to that observed at Earth should develop, with magnetic field lines and the current sheet oriented approximately parallel to the solar wind flow and with the current flowing in a $\theta$-shaped pattern across the magnetotail from one side to another and returning along the magnetopause above and below. What is in dispute is not the existence of such a structure but the distance



Table 11.2. *Magnetotail parameters derived from magnetopause model*

| | | Jupiter | |
|---|---|---|---|
| | Earth | V1 | V2 |
| Distance to subsolar point, $x_s$ | 10.9 $R_E$ | 57 $R_J$ | 68 $R_J$ |
| $\cos^2\psi$ | | | |
| at $x = -x_s$ | 0.20 | 0.27 | 0.16 |
| $x = -1.5x_s$ | 0.17 | 0.23 | 0.13 |
| $-\nu_T \equiv \partial \log B_T / \partial \log \lvert x\rvert$ | | | |
| at $x = -x_s$ | 0.20 | 0.18 | 0.23 |
| $x = -1.5x_s$ | 0.25 | 0.21 | 0.26 |

where it begins. In a terrestrial-type magnetotail, the pressure of the magnetic field $B_T$ in the lobes above and below the current sheet must equal the pressure $P_{MS}$ of the solar wind plasma in the adjacent magnetosheath, which is given fairly adequately by the Newtonian approximation

$$B_T^2/\mu_0 = P_{MS} = 0.9\,P_{SW}\,(\cos^2\psi + \epsilon) \tag{11.162}$$

where $\psi$ is the angle between the upstream solar wind flow direction and the normal to the magnetopause, $P_{SW}$ is the solar wind dynamic pressure, and $\epsilon << 1$ is the ratio of the thermal to the dynamic pressure in the upstream solar wind [see, e.g., Spreiter, Alksne, and Summers, 1968]. The magnetic field gradient with distance $-x$ down the magnetotail is then given by

$$-\nu_T \equiv \partial \log B_T/\partial \log |x| = (1/2)\,(\partial \cos^2\psi/\partial \log |x|)/(\cos^2\psi + \epsilon) \tag{11.163}$$

and can be calculated from $\cos^2\psi$ given by a model for the magnetopause surface. Table 11.2 shows some values of $\cos^2\psi$ and $\nu_T$ calculated from the parabolic models of the V 1 and V 2 magnetopause crossings given by Lepping, Burlaga, and Klein [1981] (also in Chap. 1, Sec. 1.4), together with values from a similar model for the terrestrial magnetopause given by Fairfield [1971]. (It is obvious that $\epsilon$ is small enough to be neglected in comparison to $\cos^2\psi$.) The predicted values are very similar for both the terrestrial and the Jovian magnetospheres, but whereas the observed $\nu_T \approx 0.3$ at Earth [Behannon, 1968] is slightly larger than but close to the predicted values, at Jupiter the observed field magnitude gradient [Behannon, Burlaga, and Ness, 1981; also Chap. 1, Sec. 1.4] corresponds to values of $\nu_T$ ranging from 1.4 to 1.7, larger than the predicted values by a factor between 5 and 8; furthermore, at Jupiter the observed field magnitude depends on the radial distance $r$ rather than the distance $-x$ along the solar wind flow direction. From the values of $\cos^2\psi$ one expects the observed magnetic pressure to be a fraction 1/4 to 1/8 of the solar wind dynamic pressure, but the two are nearly comparable over the 40–80 $R_J$ segments of the V 1 and V 2 outbound passes, as pointed out by Vasyliunas and Dessler [1981]. The observed field magnitude and especially its gradient thus seem to be in quantitative disagreement with the hypothesis that either Voyager 1 or Voyager 2 reached a fully developed terrestrial-type magnetotail.

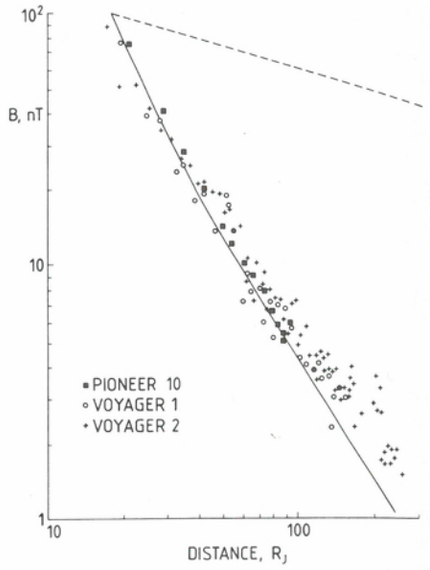


Fig. 11.18. Magnetic field magnitude observed during the Pioneer 10 and Voyager 1 and 2 outbound passes [after Behannon, Burlaga, and Ness, 1981, with omission of P 10 values beyond the magnetopause at 98 $R_J$). Solid curve: $B$ calculated from the Goertz et al. [1976] model for $B_r$ together with the dipole field and with $B_\phi$ given by Equations (11.107) and (11.110). Dotted curve: $B \sim 1/r^{0.3}$.

The observed field magnitude as a function of radial distance for the Pioneer 10 and Voyager 1 and 2 outbound pass is shown in Figure 11.18 (the same data as in Figure 1.30 but plotted on a common scale and with P 10 values beyond the magnetopause at 98 $R_J$ omitted). To be noted is the good agreement of all three spacecraft over their common distance range $r < 98\ R_J$, indicating that the field magnitude in the midnight-to-dawn quadrant is nearly independent of local time (and thus in particular is a function of $r$ and not of $x$, as already mentioned), but also a slight but definite decrease of slope for $r > 100\ R_J$, although not to a value anywhere near $\nu_T \approx 0.3$ yet. (This decrease together with the increasing radial range of the observations may account at least in part for the progressive flattening of the power-law fits from P 10 to V 1 to V 2 reported by Behannon, Burlaga, and Ness [1981].) The flattening is larger than that expected from $(B_\phi^2 + B_r^2)^{1/2}$ with $B_\phi$ given by Equation (11.110) and $B_r \sim 1/r^{1.7}$ and may very well signify that V 1 and V 2 were at least approaching the expected terrestrial-type magnetotail with its slowly varying ($B_T \sim 1/|x|^{0.3}$) field.

The fact that the solar wind flow direction is very nearly perpendicular to Jupiter's rotation axis may make it difficult to distinguish between rotational and solar-wind-related effects by purely geometrical arguments: a vector parallel to the solar wind flow is also parallel to the rotational equator. The most reliable geometrical indicator of a solar wind influence is a dependence on local time. The magnetosphere within the midnight-to-dawn sector, out to a distance of at least 100 $R_J$, appears to be remarkably independent of local time [Vasyliunas, 1982a]: the ratio $B_\phi/B_r$, the magnetic field magnitude, and the effective radial propagation speed for the shape of the current sheet all show little or no significant difference between the outbound passes of Pioneer 10 and Voyager 1 and 2. By contrast, there are clear local-time variations observed within the dawn-to-noon sector; between P 10 outbound near dawn and P 11 outbound near noon, the azimuthal sheet current density as indicated by $B_r$ decreases by about a factor of 3 [Jones, Thomas, and Melville, 1981]. Detailed models of such effects and their physical interpretation remain to be developed. As discussed already in Section 11.3.4, a crucial test for rotational vs. solar-wind effects should be provided by observations (if and when they are obtained) within the duskside of the magnetosphere.



## 11.4. Plasma flow models

### 1. General principles

The rest of this chapter presents a brief summary of models for the plasma flow in the magnetosphere of Jupiter. The brevity is imposed primarily by limitations of chapter length, although it is also true that both observation and theory are far less extensively developed for the flow than for the magnetic field and plasma distribution. Available observations of the flow are reviewed in Chapters 3 and 4.

The formulation of the basic physical principles governing the flow is contained in the theory of magnetosphere–ionosphere interaction, extensively developed and applied in the case of the terrestrial magnetosphere [see, e.g., Vasyliunas, 1970, 1972a, 1975c; Boström, 1974; Wolf, 1974, 1975, and references therein]. Within the magnetosphere, the electric field $\mathbf{E}$ and the plasma bulk flow velocity $\mathbf{V}$ are connected by the MHD relation, Equation (11.118) (see, e.g., Vasyliunas [1975a] for a discussion of its applicability and limitations). Within the ionosphere, the height-integrated current density $\mathbf{j}'$ is given by

$$\mathbf{j}' = \Sigma(\mathbf{E} + \mathbf{V}_n \times \mathbf{B}) \tag{11.164}$$

where $\Sigma$ is the height-integrated conductivity and $\mathbf{V}_n$ the velocity of the neutral atmosphere at ionospheric altitudes. Because of the thinness of the ionosphere compared to 1 $R_J$, the horizontal electric field is essentially independent of height up to and including the lowest regions of the magnetosphere just above the ionosphere; hence, comparing Equations (11.118) and (11.164) we have

$$\mathbf{j}' = \Sigma(\mathbf{V}_n - \mathbf{V}) \times \mathbf{B} \tag{11.165}$$

where $\mathbf{V}$ is the plasma velocity just above the ionosphere. Nonzero horizontal ionospheric currents exist if and only if the plasma velocity just above the ionosphere differs from the velocity of the neutral atmosphere within the ionosphere. A nonzero divergence of $\mathbf{j}'$ gives rise to Birkeland (magnetic-field-aligned) currents between the ionosphere and the magnetosphere; these currents then close through $\mathbf{j}$ perpendicular to $\mathbf{B}$ in the equatorial regions, subject to the momentum Equation (11.1) and the stress balance considerations discussed in Section 11.2.

Well-known consequences of Equation (11.118) are that the magnetic flux through any loop moving with the plasma remains constant and that plasma elements initially on a magnetic field line remain on a field line [see, e.g., Stern, 1966; Vasyliunas, 1972b]. Hence, for a given magnetic field configuration, the plasma velocity $\mathbf{V}$ just above the ionosphere, at the foot of a magnetic field line, determines $\mathbf{V}$ perpendicular to $\mathbf{B}$ everywhere along the field line. The component of $\mathbf{V}$ parallel to $\mathbf{B}$ is governed by continuity and stress balance along $\mathbf{B}$ and is less easily determined. The large size of the Jovian magnetosphere implies that the timescale to establish equilibrium along $\mathbf{B}$ may be comparatively long, and some flow observations have been interpreted as parallel flows related to this effect [Belcher and McNutt, 1980; Chap. 3].

### 2. Corotation

If the ionospheric conductivity $\Sigma$ is very large, Equation (11.165) implies that $\mathbf{V} = \mathbf{V}_n$, that is, the magnetospheric plasma moves with the neutral atmosphere. This is the motion that is meant when one speaks of the corotation of magnetospheric plasma, since $\mathbf{V}_n \approx \Omega_J \times \mathbf{r}$ to an accuracy adequate for most purposes. Note that: (1) corotation refers to motion of the plasma and not of the magnetic field pattern as

such – dipole tilt or another longitudinal asymmetry of the field is neither necessary nor sufficient for corotation; (2) the plasma moves with the upper neutral atmosphere and not with the planetary rotation except insofar as it is imposed on the atmosphere. (Strictly speaking, the corotation frequency is that of System I or II, depending on latitude, and not of System III, although the differences between them are far smaller than the actual differences between $\mathbf{V}$ and $\mathbf{V}_n$.)

If the plasma flow in the magnetosphere is to be at least approximately azimuthal with the angular velocity of planetary rotation, four conditions must be met: (1) sufficiently effective vertical transport of momentum in the atmosphere to maintain corotation of the neutral atmosphere at ionospheric altitudes (planet-atmosphere coupling); (2) high ionospheric conductivity (atmosphere-ionosphere coupling); (3) validity of the MHD approximation (11.118) (ionosphere-magnetosphere coupling); and (4) adequate magnetic stresses to balance the centripetal acceleration of the plasma.

(1) That condition (1) is satisfied is generally taken for granted by magnetospheric physicists, although Kennel and Coroniti [1975] have expressed some doubts.

(2) The value of $\Sigma$ needed for $\mathbf{V} \approx \mathbf{V}_n$ increases in direct proportion to mechanical stresses in the magnetosphere (or at its boundary) that tend to oppose or modify the corotational motion of the plasma, since these stresses must balance the $\mathbf{j} \times \mathbf{B}$ force associated with the magnetospheric closure of currents proportional to $\Sigma(\mathbf{V}_n - \mathbf{V})$ [see Eq. (11.165)]. Specific examples are discussed in Sections 11.4.4, 11.4.5, and 11.4.6.

(3) As a rule, the MHD approximation is valid for structures with length scales much larger than all microscopic lengths (gyroradii, etc.) of the plasma [see, e.g., Vasyliunas, 1975a]. Within the Earth's magnetosphere, the MHD approximation provides a good description of nearly all global and intermediate-scale features [see, e.g., Vasyliunas, 1976], a conclusion that holds a fortiori for the Jovian magnetosphere with its even larger size.

These three conditions suffice to make the components of the plasma flow perpendicular to $\mathbf{B}$ correspond to corotational motion. It is, however, still possible for $\mathbf{V}$ in the magnetosphere to deviate significantly from azimuthal motion as a result of flow parallel to $\mathbf{B}$ or of time variations of $\mathbf{B}$. To preclude this, condition (4) is necessary. Its specific requirements have been discussed in detail in Sections 11.2.2, 11.3.1, and 11.3.2.

The defining characteristic of corotation is that plasma at the foot of each magnetic flux tube circles about the rotation axis (not the dipole axis); the perpendicular flow throughout the rest of the magnetosphere is then determined by tracing the magnetic field lines attached to the moving plasma. If there are significant distortions of the magnetic field lines that depend on local time (or, more generally, are not time-independent when viewed from a corotating frame of reference), the resulting motion in the equatorial plane may deviate considerably from simple azimuthal flow. In particular, if field lines are extended on the nightside and compressed by the solar wind on the dayside, as expected for the outermost regions of the magnetosphere, corotational motion has not only azimuthal but also radial components in the equatorial plane, inward on the dawnside and outward on the duskside. Such a flow is crucial for the acceleration mechanism proposed by Goertz [1978] (see also Chap. 10, Sec. 6).

### 3. Radial outflow and planetary/magnetospheric wind

There is a limit to the distance at which a flux tube of given plasma content can be maintained in rigid corotation by an inward magnetic stress. It is often stated that at the limiting distance the Alfvén speed equals the corotation speed, but in fact that gives only an order-of-magnitude estimate; the actual value of the limiting distance is set by



the tangential stress balance (Secs. 11.2 and 11.3). For the Gleeson–Axford and the Hill–Carbary models discussed in Section 11.3.1, the limiting distance is given by the (virtually identical) Equations (11.68) and (11.74). (It may be noted that, with the assumptions of plasma sheet thickness $h \approx r$ and mass density $\rho \sim 1/r^4$, appropriate to an ionospheric plasma source in a dipolar field assumed by Hill, Dessler, and Michel [1974] and Michel and Sturrock [1974], these equations predict a limiting distance larger by only a factor of 1.2 than the distance given by the simple $V_A = \Omega r$ estimate.) Corotation out to a considerably larger distance is seemingly allowed by the magnetic field model of Goertz et al. [1976], but this is possible only because either the flux tube content or the corotation speed implied by the model decreases with increasing distance, as shown in Section 11.3.2.

If, then, plasma on a magnetic flux tube is transported outward beyond the limiting distance and neither the flux tube content nor the corotation frequency of the ionosphere are allowed to decrease, the plasma will begin to move in a path approaching a straight line, unless deflected by stresses other than the now too small magnetic tension. On the dayside, the constraint of remaining within the magnetosphere may force the plasma to continue moving in a curved path similar to corotation, with solar wind pressure on the magnetopause providing the necessary inward stress, but on the nightside the plasma may move nearly freely outward into the low-pressure, low-density magnetotail; the magnetic field lines, attached to the corotating ionosphere at one end and to the outward-flowing plasma at the other, become highly extended and eventually break open. This is the concept of rotationally driven plasma radial outflow described by Hill, Dessler, and Michel [1974] and Michel and Sturrock [1974], named by them the planetary wind. Figure 11.19 shows a sketch of the expected flow pattern in the equatorial plane and the associated topological changes of the magnetic field. The extended magnetic field lines become detached through the formation of singular lines of $\times$ and $\bigcirc$ type (see Vasyliunas [1976] and references therein, for a discussion of analogous topological changes in the terrestrial magnetotail). At the $\times$ line, a magnetic-merging process [e.g., Vasyliunas, 1975a] is expected to occur, with consequent flow pattern as shown in Figure 11.19, plasma heating, and particle acceleration [Carbary, Hill, and Dessler, 1976; Chap. 10, Sec. 6]. The precise expected location of the $\times$ and $\bigcirc$ lines is at present unknown (although an alignment of the $\bigcirc$ line with the plasma flow is implied by the results of Vasyliunas [1980]), and the locations shown in Figure 11.19 are a free sketch.

There is a strong qualitative similarity between the flow pattern of Figure 11.19, expected on the basis of the planetary wind model, and the flow pattern inferred from Voyager charged particle observations [Krimigis et al., 1979b, their Fig. 9; Chap. 4, Fig. 4.7]. The radial outflow observed by Krimigis et al. and named by them the magnetospheric wind may thus be plausibly identified with the planetary wind, specifically with the expected strong tailward flow beyond the $\times$ line near the dawn magnetopause.

The planetary-wind model as such makes no predictions about either the source or the temperature of the plasma – these must be provided as inputs, and the assumption of a cold ionospheric plasma in Hill, Dessler, and Michel [1974] and Michel and Sturrock [1974] is not part of the model but simply the pre-Voyager prevailing view. The limiting distance, beyond which radial outflow should begin, given by Equation (11.74) with the use of Voyager determinations of the plasma mass density $\rho$ and the plasma sheet thickness $h$, is 24 $R_J$ (the value of about 10 $R_J$ given in Chap. 4 results from using $\rho$ but ignoring $h$ and tacitly assuming that the plasma sheet extends over the entire flux tube), but this estimate presupposes rigid corotation of the ionosphere at all latitudes, which is almost certainly not the case (see Secs. 11.3.4 and 11.4.4); allowance

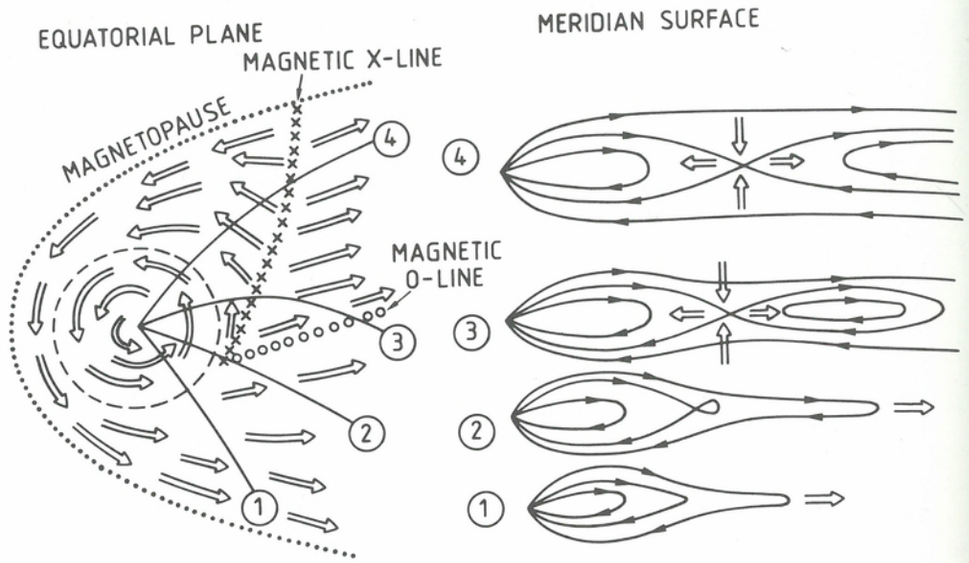


Fig. 11.19. Qualitative sketch of plasma flow in the equatorial plane (left) and of the associated magnetic field and plasma flow in a sequence of meridian surfaces (right) expected from the planetary wind model. The locations of the × and ○ lines are speculative but have *not* been adjusted to take account of any observations (they are identical to the pre-Voyager locations drawn by Vasyliunas in 1978 for a conference presentation but not published; thus this figure and Fig. 9 of Krimigis et al. [1979b] are independent).

of partial corotation will, of course, increase the limiting distance. Furthermore, it is apparent from Figure 11.19 that strong radial outflow in the predawn sector is expected only beyond the × line, as a result of superimposed flows from magnetic merging.

If the solar wind pressure is reduced and the magnetopause recedes to great distances, it is possible for radial outflow and the associated formation of magnetic loops to occur at all local times. Models with such an axially symmetric planetary wind as well as possible transitions between symmetric and nightside-only outflow in response to solar wind pressure changes have been considered by Kennel and Coroniti [1977a] and Coroniti and Kennel [1977] but have not received much observational support.

The distinction between the rotationally driven stellar wind model of Mestel [1968] and the planetary wind model is not always clearly made [Kennel and Coroniti, 1977a; Goertz, 1979]. The Mestel model describes radial outflow along open magnetic field lines, with a plasma source at the inner end (i.e., the ionosphere) and vanishing pressure at large distances; by contrast, the planetary wind model has field lines that for the most part are either closed or form detached loops, radial outflow perpendicular to the magnetic field in the equatorial plane, and plasma that is concentrated toward the equatorial regions. The Mestel model has a critical Alfvén radius $r_A$, with near-corotation of plasma for $r << r_A$ and super-Alfvénic outflow for $r >> r_A$, but this is a transition within a single (open) flux tube, not a limiting distance in the equatorial plane; furthermore, $r_A$ is defined by the condition $B_r^2/\mu_0 \rho = V_r^2$, where $V_r$ is the radial outflow and not the corotational speed, and thus differs from both the precise and the



order-of-magnitude expressions for the limiting distance of the planetary wind model. It is possible that a Mestel-type outflow may exist, on the open field lines within the Jovian magnetosphere well above the current sheet, as a rotationally driven species of polar wind [cf. Fig. 2 of Hill, Dessler, and Michel, 1974] distinct from the planetary/magnetospheric wind.

### 4. Partial corotation

With outward transport of plasma from a source within the inner magnetosphere, corotation requires a magnetic torque exerted by radial currents which close through the ionosphere (see Sec. 11.3.4). Hill [1979] pointed out that the difference between the plasma and the neutral atmosphere velocities required to drive these currents [see Eq. (11.165)] leads to a reduction of the azimuthal plasma flow speed in the ionosphere and therefore also in the magnetosphere, that is, a partial corotation of the plasma, with angular frequency $\omega < \Omega_J$. The theory of partial corotation combines two aspects already considered in detail separately in Section 11.3.4: the relations of $B_\phi$ to the ionospheric current, leading to Equation (11.129), on the one hand, and to the torque on the plasma, Equation (11.134), on the other. Elimination of $B_\phi$ between these two equations yields a differential equation for $\omega$ as a function of $r$, which was derived by Hill without explicit consideration of $B_\phi$. With the meridional magnetic field approximated by a dipole, Hill showed that $\omega$ decreases gradually, falling appreciably below $\Omega_J$ at a characteristic distance $r_c$ given by

$$(r_c/R_J)^4 = \pi \Sigma B_J^2 R_J^2/S \tag{11.166}$$

where $S$ is the net outward mass flux; for $r >> r_c$,

$$\omega \approx \pi^{1/2} \Omega_J (r_c/r)^2 \tag{11.167}$$

corresponding to negligible torque on the plasma. Numerically,

$$r_c = [(\Sigma/1 \text{ mho}) (10^{30} \text{ amu/s})/S]^{1/4} 36 R_J \tag{11.168}$$

From a comparison with Voyager 1 observations, Hill [1980] estimated $r_c \approx 20 R_J$. (The comparison requires some care because $\omega$ given by the theory is actually the radial-flux-weighted average $\langle \omega \rangle$ defined in Equation (11.135).) The model of $B_\phi$ discussed by Vasyliunas [1982b] and in Section 11.3.4 identifies the radial currents implied by the observed $B_\phi$ with those responsible for partial corotation in Hill's model.

The characteristic distance $r_c$, beyond which there is no rigid corotation because condition (2) of Section 11.4.2 (atmosphere–ionosphere coupling) is not satisfied, is entirely distinct from the limiting distance $r_0$, given in Equation (11.74) and discussed in Section 11.4.3, beyond which condition (4) (centrifugal stress balance) is not satisfied. [Equation (11.74) is applicable only if $r_0 \lesssim r_c$, because rigid corotation of the ionosphere was assumed in deriving it.] The ratio $r_c/r_0$ is given by

$$(r_c/r_0)^4 = \pi \mu_0 \Sigma \rho_s h_s \Omega_J^2 L_s^3/4S \tag{11.169}$$

which can be written as

$$(r_c/r_0)^4 = \mu_0 \Sigma (\Omega_J r_s)^2/8 \langle V_r \rangle \tag{11.170}$$

where $\langle V_r \rangle$ is the average speed of radial transport out of the Io torus defined by

$$S = 2\pi r_s \rho_s h_s \langle V_r \rangle. \tag{11.171}$$

Empirical estimates give a ratio $r_c/r_0$ close to one. Whether this is merely a remarkable coincidence or whether the outward transport process adjusts $\langle V_r \rangle$ to give this value is an interesting unanswered question.

The angular frequency of corotation, whether rigid or partial, of the ionospheric and magnetospheric plasmas has no direct connection with the periodic modulation of Jovian radio emissions (see Chapters 7 and 9). The modulation implies that the spatial configuration of the emission sources has some azimuthal asymmetry, and it is the effective rotation of this asymmetric spatial pattern that determines the modulation period. For example, the modulation is at Jupiter's rotation period if the asymmetry is associated with dipole tilt or magnetic anomaly effects and at Io's orbital period if it is associated with the Io flux tube, regardless of what the plasma motions are. If the Jovian magnetosphere were axially symmetric in all respects, there could be no periodic modulation of the radio emissions but the physics of corotation and its limits would not be changed in any substantial way.

Effects analogous to partial corotation, associated with azimuthal stresses produced by inward and outward motions that result from day–night asymmetries or from compressions and expansions of the magnetosphere, have been considered by Nishida and Watanabe [1981].

### 5. Solar-wind-driven magnetospheric convection

Plasma flow analogous to magnetospheric convection at Earth, induced by the flow of the solar wind past the magnetosphere, is discussed in Chapter 10, Section 2 and shown to be of little importance at Jupiter.

### 6. Corotating magnetospheric convection

One of the main tenets of the magnetic anomaly model is an enhancement of the plasma content within the Io torus over the longitude range of the active sector (see Chap. 10 for a detailed discussion). The corotation of the plasma implies a corresponding enhancement of the centrifugal stress and hence of the balancing $\mathbf{j} \times \mathbf{B}$ force. Because the enhanced azimuthal current is confined to the active sector, continuity requires it to couple to Birkeland currents at the edges of the active sector, with current closure through the ionosphere [see, e.g., Dessler, 1980a]. Vasyliunas [1978] pointed out that the electric field (or, equivalently, the difference between the plasma and the neutral atmosphere velocities) required to drive the closing ionospheric currents implies a two-cell pattern of circulating plasma flow, with outward flow over the active sector and inward flow at other longitudes. The flow pattern is stationary when viewed from a frame of reference rotating with the planet, rather like an atmospheric cyclonic feature (the ionospheric projection of the flow has the appearance of four huge eddies, two in each hemisphere, with their centers at approximately 90° longitude to each side of the active sector); it thus differs from solar-wind-driven magnetospheric convection, which is also basically a two-cell circulating flow but fixed in local time rather than in System III longitude. The mean speed of the flow or equivalently the characteristic circulation frequency scales as the ratio of mass content asymmetry in the Io torus to the ionospheric conductivity. Limited quantitative models have been developed by Hill, Dessler, and Maher [1981] and by Summers and Siscoe [1982], and possible applications to various observed phenomena are discussed by Hill, Dessler, and Maher [1981] and by Dessler, Sandel, and Atreya [1981] (see also Chap. 10, Section 7).



### 7. Radial diffusion

There are several mechanisms by which plasma circulatory motions may arise that are somewhat similar to magnetospheric convection (either corotating or solar-wind driven) but are transient and variable in time and/or longitude rather than stationary; they may also have much smaller scales, with many small cells instead of two large ones. One mechanism is the centrifugal instability of the Io torus, which is in effect an unsteady succession of corotating magnetospheric convection patterns, produced not by a fixed asymmetry but by random enhancements of the plasma content (which grow as a consequence of the flow). Another is the coupling of ionospheric plasma flow to circulatory motions of the neutral atmosphere, with $\mathbf{j}' = 0$ and $\mathbf{V} = \mathbf{V}_n$ in Equation (11.165). Radial diffusion is the transport of plasma and energetic particles that results from the averaging over such stochastic circulatory motions. Historically, atmospheric winds were the first to be suggested as the mechanism of radial diffusion in the Jovian magnetosphere [Brice and McDonough, 1973]. For a detailed discussion of radial diffusion driven by centrifugal effects of the Io torus, see Siscoe and Summers [1981] and references therein. The mathematical description of the transport by radial diffusion, largely independent of the specific mechanism, is discussed in Chapter 5. Its application to the plasma distribution is considered by Siscoe [1978b]; for application to radiation belt particles, see, for example, Schulz [1979] and Chapter 5.

## 11.5. Conclusion

The dominant structure of the Jovian magnetosphere, the extended near-equatorial sheet of plasma and electric current, is fairly well understood at least qualitatively in physical terms of stress balance between the plasma and the magnetic field, but a number of aspects need further quantitative development and others remain with some basic physical questions unanswered. There is for the most part an order-of-magnitude agreement between the observed plasma parameters and those implied by stress balance with the observed magnetic field, but few detailed comparisons have been carried out as yet. The plasma density implied by stress balance depends rather sensitively on the assumed field model; purely empirical fits to the observed magnetic field without taking into account any self-consistency requirements are liable to yield models that imply some unphysical properties for the plasma. There is continuing controversy on the relative importance of rotational vs. solar wind effects in the outermost regions of the magnetosphere, in particular for the interpretation of local time variations or lack of them; the range of viable alternatives would be greatly narrowed by even limited observations from the so far unexplored duskside. Both direct observations and inferences from field-plasma self-consistency indicate that the azimuthal flow of the plasma decreases well below rigid corotation at large distances at least on the nightside, an effect that is well understood theoretically and can be quantitatively related to the observed azimuthal magnetic field. Understanding of plasma flow other than partial corotation remains fragmentary, and the nature of the outward radial transport mechanism – convection or diffusion, and the ratio of net outflow to circulating mass flux – has not been firmly established.

## APPENDIX: COMMENTS ON SOME MAGNETIC FIELD MODELS

(1) The model of Vickers [1978] is intended as a generalization of the Gleeson–Axford model to include a radial pressure gradient. In the radial stress balance equation

$$-\rho\omega^2 r + \partial P/\partial r = B_z(\partial B_r/\partial z)/\mu_0 \qquad (11.172)$$

[equivalent to (11.15) with isotropic pressure, centripetal acceleration, and $B_p = B_r$], one may set (in our notation) $\rho = P/w^2$ and $P = (B_0^2 - B_r^2)/2\mu_0$ given by pressure balance ($B_0 \equiv B_p^*$ is the field outside the current sheet), and solve for $B_z$ to obtain

$$B_z = [(\partial/\partial r)(B_0^2 - B_r^2) - (\omega^2 r/w^2)(B_0^2 - B_r^2)]/2\,(\partial B_r/\partial z) \tag{11.173}$$

If we assume that $B_r$ has the form

$$B_r = B_0(r) \tanh (z/h) \tag{11.174}$$

then the RH side of (11.173) is independent of $z$ and

$$B_z = [dB_0/dr - \omega^2 r B_0/2w]\, h \tag{11.175}$$

provided *either* $h$ is independent of $r$ *or* the radial pressure gradient term (and hence $dB_0/dr$) is neglected entirely. Gleeson and Axford [1976] choose the second alternative; then $h$ is in general a function of $r$, and Equation (11.175) with $dB_0/dr$ omitted becomes simply an expression for the current sheet thickness in terms of field and thermal quantities, identical in fact to Equation (11.99) with $\mu >> 1$. Vickers, however, retains the pressure gradient term and argues that $B_r$ given by (11.174) with constant $h$ is a general solution because $B_z$ given by (11.175) gives $\partial B_z/\partial z = 0$ in agreement with $\nabla \cdot \mathbf{B} = 0$ for a thin sheet; with both $B_z$ and $B_0$ related to the current density $j_\phi'(r)$, an integrodifferential equation for $j_\phi'$ is obtained which has a unique solution, in contrast to the freedom of Gleeson and Axford to choose $j_\phi'$ arbitrarily.

The apparent uniqueness of the solution is simply a consequence of the assumed constant thickness h and otherwise has no direct connection with inclusion of the radial pressure gradient. It would be possible to assume $h$ = constant and use Equation (11.175) without $dB_0/dr$ to obtain a unique $j_\phi'$ for the Gleeson–Axford model. In fact, there is no basis for assuming a strictly constant $h$, and the argument given by Vickers is incorrect: from $\nabla \cdot \mathbf{B} = 0$ and $B_r$ given by (11.174), it is readily shown that

$$B_z(r, z) = B_z(r, 0) - h(dB_0/dr + B_0/r) \log \operatorname{sech} (z/h) \tag{11.176}$$

so that Equation (11.175) is *not* satisfied unless $dB_0/dr = 0$ and $h/r \to 0$ because one side depends on $z$ and the other does not. Equation (11.174) thus does not give a solution except in the Gleeson–Axford limit of negligible radial gradient and $h << r$ an unspecified function.

(2) The model of Barish and Smith [1975] is intended to illustrate how the stretched-out magnetic field lines can nevertheless close within the compressed dayside magnetosphere and to represent the Pioneer 10 inbound magnetic field observations. Actually, it fulfills neither purpose. As to the comparison with observations, the model has nearly radial field lines in the outer magnetosphere which reverse across the current sheet; hence, it predicts a strong 10-hr modulation to be observed by Pioneer 10 as the current sheet sweeps up and down past the spacecraft. In fact, the striking feature of the Pioneer 10 observations between 95 $R_J$ and 55 $R_J$ inbound is that the magnetic field was more nearly normal to the equatorial plane and showed little evidence of 10-hr modulation [Smith et al., 1976, especially their Fig. 5].

As to the intended closure of field lines, the magnetic flux function of the model in the equatorial plane may be written as $f = M\alpha$, where $M$ is the Jovian dipole moment and $\alpha$ is given by

$$\alpha^5(\alpha - \alpha_d) - \epsilon \log (R/r) = 0 \tag{11.177}$$

where $\alpha_d = 1/r$ describes a dipole field, $\epsilon = 1.623 \times 10^{-10}\, R_J^{-6}$, and $R = 100\, R_J$ (see



also Chap. 1, Sec. 1.3). It is easily shown that for $r \leq R$ Equation (11.177) has two real solutions $\alpha_1$ and $\alpha_2$, with $\alpha_1 = 0$ and $\alpha_2 = \alpha_d$ at $r = R$. From Equation (11.177) it is then obvious that $\alpha_1 \leq 0$ and $\alpha_2 \geq \alpha_d$ for all $r \leq R$, and it can further be shown that $d\alpha_1/dr > 0$, whereas $d\alpha_d/dr < 0$; thus $\alpha_1$ must be rejected because it represents a magnetic field with $B_z$ opposite in sign throughout the magnetosphere to the field of the assumed planetary dipole (note that $\alpha$ is intended to represent not just the perturbation but the total field, including the dipole). The other solution does represent a suitable field with extended field lines, but the magnetic flux is not contained within $r = R$, the intended distance of the magnetopause, where $\alpha_2 = \alpha_d$ and thus the unclosed flux is equal to the dipole flux. It can be shown that the two solution branches come together at a distance $r = R_2 = 100.04\, R_J$, where $\alpha_1 = \alpha_2 = (5/6)\alpha_d$ and $|d\alpha/dr| \to \infty$; for $r > R_2$, Equation (11.177) has no real solutions. A fraction 1/6 of the unclosed flux at $r = R$ thus closes between $r = 100.00$ and $r = 100.04$ and the rest closes through a singular layer of zero thickness and infinite field. It may be noted that the model gives $|B_z| = 1.42\, nT$ at $r = 90\, R_J$, 2.15 $nT$ at $r = 95\, R_J$ and 68.6 $nT$ at $r = 100\, R_J$.

(3) The azimuthal current density in the model of Goertz et al. [1976] (obtained by taking the curl of the full model field as a function of $r$ and $z$) has two components: one varying as $\operatorname{sech}^2(z/D)$ and another extending over a wide latitude range and depending only on $z/r$ when $|z| >> D$. The first evidently represents the actual current sheet and the second is usually ignored; it may be an artifact resulting from specifying both $B_z$ and $B_r$ at the current sheet (assumption of $\nabla \times \mathbf{B} = 0$ outside the current sheet would give a boundary value problem whose solution determines $B_z$ given $B_r$ or vice versa). In computing the pressure from vertical stress balance in the model, there is thus some ambiguity as to where $P$ should be set to zero, since $j_\phi \neq 0$ at all finite distances. In Section 11.3.2, only the field associated with the $\operatorname{sech}^2 z/D$ component was included in the pressure balance. Goertz et al. [1979], on the other hand, set $P = 0$ at the last closed field line, and Goldstein [1977] treats the pressure in the equatorial plane as a boundary condition to be specified by an independent assumption.

## ACKNOWLEDGMENTS

I am grateful to A. J. Dessler, T. W. Hill, W. I. Axford, C. K. Goertz, H. Goldstein, G. Burgess, and J. E. P. Connerney for useful comments on the manuscript and to J. E. P. Connerney for providing a table of calculated field values from the Connerney-Acuña-Ness model.